ABSTRACT

Title of Document: THERMO-MECHANICAL DESIGN STUDY OF FIBER OPTIC PRESSURE SENSOR DIAPHRAGMS.

Yasir Majeed, Master of Science,

Mechanical Engineering, 2009

Directed By: Professor Abhijit Dasgupta,

Department of Mechanical Engineering

This thesis parametrically explores the nonlinear design sensitivity of a fiber optic pressure sensor (FOPS), based on selected thermo-mechanical failure mechanisms expected in the sensor diaphragm. The product under study is a miniature FOPS that can be embedded in, or installed on, a structure for pressure monitoring applications. The field operating conditions considered in this study are defined in terms of temperature and pressure The FOPS probe has a Fabry-Perot cavity, with the fiber tip and a miniature diaphragm acting as the two mirrors. The cavity length changes when the diaphragm deflects under pressure. However, due to field operating conditions,

several failure mechanisms may affect the structural and optical characteristics of the sensor, such as nonlinear displacement of the diaphragm, cracks in the diaphragm, buckling of the diaphragm, high residual stresses in the optical fiber and deformations and failure in the epoxy sealant between the optical fiber and the steel casing. With the aid of nonlinear thermomechanical finite element analysis, this article investigates conflicting design constraints due to sensitivity and selected failure mechanisms in the sensor, e.g. nonlinear diaphragm deformation, diaphragm fracture and diaphragm buckling.

The study is divided into three parts. The first part of this study considers the mechanical loading due to external pressure which the FOPS will experience and gives design guidelines based on the nonlinear diaphragm deflection and stress predictions. The second part accounts for the thermo-mechanical loading in which the FOPS is placed in a temperature drop and the resulting nonlinear in-plane compressive stresses and diaphragm deflections are analyzed. In the third part of this study the combined effects of pressure and thermal loadings are examined for more realistic application conditions. Design guidelines for both simultaneous and sequential changes in temperature and pressure are examined, to represent different working environments.

THERMO-MECHANICAL DESIGN STUDY OF FIBER OPTIC PRESSURE SENSOR DIAPHRAGMS

By

Yasir Majeed

Thesis submitted to the Faculty of the Graduate School of the
University of Maryland, College Park, in partial fulfillment
of the requirements for the degree of
Master of Science
2009

Advisory Committee:

Professor Abhijit Dasgupta, Chair

Dr. Hugh Bruck

Dr. Miao Yu

Dr. Moustafa Al-Bassyiouni

Dedication

To my mother and father

Acknowledgements

Ever since grade school, the desire to obtain a higher degree in engineering has been pivotal in my life and this desire has been omnipresent in every decision I have ever made. The importance I have placed on my education stems from the fact that I come from a family where no one had the opportunity to get an education at higher level. Fortunately for me, my family has been my light to guide me through good times and bad. I would like to thank my parents and sisters and their families for their tremendous unconditional love and support.

I am also extremely thankful for the day I was passing by the Interconnects research lab and saw a flyer on the door asking students to apply for an undergraduate research position. Had it not been for that flyer, I would have not had the opportunity to work with Dr. Abhijit Dasgupta as an undergraduate and then a graduate student. I would like to thank him for all his guidance and support, without which I will not be where I am now. I would also like to thank Dr. Moustafa Al-Bassyiouni for being a great mentor and assisting me at every point and turn.

Table of Contents

List of Figures

Chapter 1: Introduction

In dynamic pressure sensors, the dynamic pressure is usually detected through the displacement of a thin diaphragm. In this study, the diaphragm displacement is detected with a fiber optic sensor. Fiber Optic Pressure Sensors (FOPS) are becoming increasingly popular because of their high sensitivity and low sensitivity to electromagnetic interference. The sensing is based on detecting the optical phase change induced in the light as it propagates along the optical fiber. Fabry-Perot sensors are a sub-category of these sensors and offer higher accuracy and better signal-to-noise characteristics than optical sensors based on Bragg gratings [16]. These sensors can measure changes in pressure, displacement and temperatures. The FOPS probe has a Fabry-Perot cavity, with the fiber tip and a miniature diaphragm acting as the two mirrors. The cavity length changes when the diaphragm deflects under pressure resulting in detectable optical phase shifts. However, due to field operating conditions, several failure mechanisms may affect the structural and optical characteristics of the sensor, such nonlinear deformation of the diaphragm, and fracture and/or buckling of the diaphragm. Sources of failure in our study are in the diaphragm due to temperature and pressure. Additional errors may occur due to fiber expansion, changes in refractive index and changes in air properties, but are not considered in this study.

Choosing a suitable diaphragm design is important for optimizing the sensor parameters because the sensitivity of the sensor is related to the behavior of the thin diaphragm. Diaphragm thickness is an important factor in the sensitivity of the sensor. As the diaphragm thickness is reduced, the sensitivity increases but at the expense of increasing the stresses and risk of fatigue damage and buckling failure under thermal stresses. Furthermore, the measurement range of the sensor decreases with thickness because of nonlinear response of the diaphragm to pressure loading. There has to be design optimization based on trade-offs between sensitivity and reliability margins. To conduct the optimization, models must be developed that quantify the sensitivity of the sensor and the reliability margins, under pressure and thermal loading. With the aid of finite element analysis, this thesis investigates the reliability of fiber optic sensor diaphragm under pressure and temperature loadings and its influence on the design optimization of the diaphragm.

1.1 Background and Literature Review

Studies have been reported in the literature to optimize FOPS diaphragm sensitivity. Shilpak and Dugungi [1] conducted static analyses of a clamped circular plate under initial tension and studied the plate behavior and when the plate transitions into a membrane/thin diaphragm in terms of tension parameter k. This transaction occurs over the range $1<k<20$. Where the behavior is that of a thin plate for $k<1$, and when $k>20$, the plate behaves like a thin membrane. Yu and Balachandran [2] studied the diaphragm response in terms of this tension parameter k and showed that the analysis and the results can be used to design a sensor diaphragm to maximize sensitivity. In

recent work [3-5] there has been emphasis on the design studies conducted in fiber optic sensors field to optimize the sensitivity of the sensors by studying the diaphragm deflection.

If the diaphragm experiences compressive radial stresses due to thermo-mechanical constraints from the sensor housing, the sensor may become unstable and out of plane buckling may occur without any external forces being present [7]. This phenomenon is known as thermal buckling, and the temperature corresponding to the critical load is called the buckling temperature [8]. Beyond this critical load, deformations are not proportional to the applied pressure, and these deformations may become considerable and may rupture the diaphragm [7]. In the previous work of Majeed et. al. [9], design margins were investigated not only for the sensitivity of the thin diaphragm but also for the stresses developed on the diaphragm, which are critical to failure and optimized the design of the same FOPS with respect to sensor sensitivity and fracture due to excessive stresses on the diaphragm. Majeed et. al. [1] put forth design margins for the optimal design of the FOPS diaphragm under external pressure loading only. In reality, the FOPS will not only be exposed to a changing pressure environment, but also a varying temperature will be a factor in the loading conditions.

1.2 Problem Statement and Objectives

The internal construction of the fiber optic pressure sensor, FOPS, under study is shown in Fig. 1-1. The point of interest in this model is the thin diaphragm circled. The FOPS must withstand environmental temperature changes in operation. When the temperature drops, the outer steel shield will shrink more than the inner silicon

probe housing and the thin silicon diaphragm. The resulting compressive radial stress in the diaphragm may cause the diaphragm to buckle as the thickness is reduced for better sensitivity. Thus the diaphragm thickness must be studied to minimize the risk of buckling. This study investigates a design margin for not only the sensitivity of the thin diaphragm but also the bending and buckling stresses developed on the diaphragm, which are critical to failure.

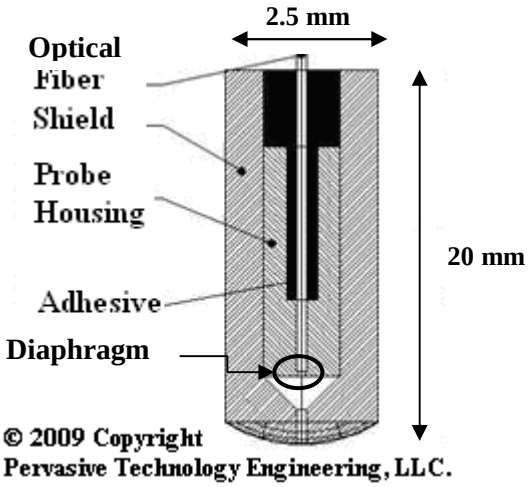

Fig. 1.1 Internal construction of the fiber optic pressure sensor (FOPS)

1.4 Organization of Thesis

This thesis is divided into three chapters following the introduction. Two of these chapters are taken directly from a paper which is being submitted for publication. Chapter 2 discusses the design optimization of FOPS under external pressure loads, both linear and nonlinear results are discusses. Chapter 3 discusses the design optimization of FOPS under external thermal loads and then a combination of

pressure and thermal loads. These discussions are followed by the conclusions in Chapter 4.

Chapter 2: Design Study of Fiber Optic Pressure Sensors at Ambient Temperature

The text of this chapter is taken from a paper that has been submitted for publication. This paper investigates the design margins under pressure loading, at ambient temperature. The measurement sensitivity and static linear operating range of the diaphragm are parametrically assessed. The stress-margins due to pressure-induced stresses in the diaphragm are also assessed. This paper is organized as follows. In Section 2.2, a linear FEA modeling approach is described. The accuracy of the model is assessed in Section 2.3 with linear analytic results. Parametric design methodology is presented in Section 2.5, followed by a nonlinear study of the operating range in Section 2.6 and conclusions in Section 2.7.

Design Study of Fiber Optic Pressure Sensors at Ambient Temperature

Yasir Majeed[1,*], Moustafa Al-Bassyiouni[1], Abhijit Dasgupta[1]

Bldg. 089, Department of Mechanical Engineering, University of Maryland, College Park, MD 20742, USA

[*]*Corresponding author: ymajeed@umd.edu*

Abstract

This paper parametrically explores the nonlinear design sensitivity and design margins of a fiber optic pressure sensor (FOPS), based on the potential failure mechanisms expected in the sensor diaphragm. The product under study is a miniature FOPS that can be embedded in, or installed on, a structure for pressure monitoring applications. The field operating conditions considered in this study are defined in terms of the operating pressure The FOPS probe has a Fabry-Perot cavity, with the fiber tip and a miniature diaphragm acting as the two mirrors. The cavity length changes when the diaphragm deflects under pressure. However, due to field operating conditions, several failure mechanisms may affect the structural and optical characteristics of the sensor, such as nonlinear displacement of the diaphragm, cracks in the diaphragm, buckling of the diaphragm, high residual stresses in the optical fiber

and deformations and failure in the epoxy sealant between the optical fiber and the steel casing. With the aid of nonlinear thermomechanical finite element analysis, this article investigates conflicting design constraints due to measurement sensitivity and selected failure mechanisms in the sensor diaphragm, eg. nonlinear diaphragm deformation, and diaphragm fracture under pressure loading. The severity of each mechanism is investigated by parametric design sensitivity studies.

Keywords: Fiber-optic pressure sensor; Fabry-Perot interferometer; nonlinear finite element analysis, parametric design optimization

2.1 Introduction

In dynamic pressure sensors, the dynamic pressure is usually detected through the displacement of a thin diaphragm. In this study, the diaphragm displacement is detected with a fiber optic sensor. Fiber Optic Pressure Sensors (FOPS) are becoming increasingly popular because of their high sensitivity and low sensitivity to electromagnetic interference. The sensing is based on detecting the optical phase change induced in the light as it propagates along the optical fiber. Fabry-Perot sensors are a sub-category of these sensors. They offer higher accuracy than any other fiber optic sensor and use broadband white-light. These sensors can measure changes in pressure, displacement and temperatures. The FOPS probe has a Fabry-Perot cavity, with the fiber tip and a miniature diaphragm acting as the two mirrors. The cavity length changes when the diaphragm deflects under pressure resulting in detectable optical phase shifts. However, due to field operating conditions, several failure mechanisms may affect the structural and optical

characteristics of the sensor, such nonlinear deformation of the diaphragm, and fracture of the diaphragm. Choosing a suitable diaphragm design is important for optimizing the sensor parameters because the sensitivity of the sensor is related to the behavior of the thin diaphragm. Diaphragm thickness is an important factor in the sensitivity of the sensor. As the diaphragm thickness is reduced, the sensitivity increases but at the expense of increasing the stresses and risk of fatigue damage and buckling failure under thermal stresses. Furthermore, the measurement range of the sensor decreases with decreasing thickness because of large nonlinear deflection of the diaphragm in response of to pressure loading. The design needs to be optimized based on trade-offs between sensitivity and reliability margins. To conduct the optimization, models must be developed that quantify the sensitivity of the sensor and the design margins, under pressure and thermal loading. With the aid of nonlinear finite element analysis, this study investigates the sensitivity and design margins of a fiber optic sensor diaphragm under pressure and temperature loadings and their influence on the design optimization of the diaphragm.

Studies have been reported in the literature to optimize FOPS diaphragm sensitivity. Shilpak and Dugungi [1] conducted static analyses of a clamped circular plate under initial tension and studied the plate behavior and when the plate transitions into a membrane/thin diaphragm in terms of a non-dimensional tension parameter k which is proportional to the square-root of the tension loading and the radius of the clamped plate, and inversely proportional to the bending stiffness of the clamped plate. This transition occurs over the range $1<k<20$. Where the behavior is that of a thin plate for $k<1$, and when $k>20$, the plate behaves like a thin membrane.

Yu and Balachandran [2] studied the diaphragm response in terms of this tension parameter *k* and showed that the analysis and the results can be used to design a sensor diaphragm to maximize sensitivity. In recent work [3-5] there has been emphasis on the design studies conducted in fiber optic sensors field to optimize the sensitivity of the sensors by studying the diaphragm deflection. This paper investigates a design margin for not only the sensitivity of the thin diaphragm but also the stresses developed on the diaphragm, which are critical to failure and buckling.

The rest of this article is organized as follows. In Section 2.2, a linear FEA modeling approach is described. Model is validated in Section 2.3 and results are presented in Section 2.4. Then the design optimization is presented in Section 2.5, followed by a nonlinear study in Section 2.6 and conclusions in Section 2.7.

2.2 FEA Model

The approach for finite element modeling of the FOPS is described in this section. Section 2.2.1 discusses the modeling of the FOPS for FEA and Section 2.2.2 discusses the material properties of the FOPS.

2.2.1 FEA Model

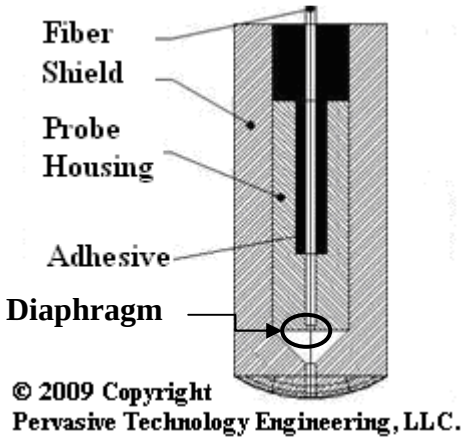

Fig. 2.1. Internal construction of the FOPS

The internal construction of the fiber optic pressure sensor (FOPS) under study is shown in Fig. 2.1. Instead of a full 3-D model, a more efficient 2-D axis-symmetric finite element model in view of the axial symmetry of the structure and loading. Details of the model are illustrated in Fig. 2.2. The point of interest in this model is the thin diaphragm circled in Fig. 2.1. In this case, there are two different types of axis-symmetric elements used. 1-D, axis-symmetric, 2-node, shell elements are used for the diaphragm and 4-noded-brick elements are used to model the rest of the FOPS body, which includes the shield, probe housing and the adhesive. The rotation of the shell elements is constrained to the brick element such that the shell element is always perpendicular to the brick element even after it has deformed. Fig. 2.2(a) shows the entire sensor under pressure loading and boundary conditions (arrows indicate the pressure loading, hash markings indicate the boundary loading condition (different materials as assigned different colors for better visualization) and Fig. 2.2(b) shows a closer view of the diaphragm. The tip of the sensor is exposed to a boundary

condition of 1 bar of pressure which also acts on the sensor diaphragm. The top is under a zero pressure boundary condition and is constrained in all three degrees-of-freedom (Fig. 2.2(a)). Symmetry condition is applied along the axis of symmetry along the axial direction.

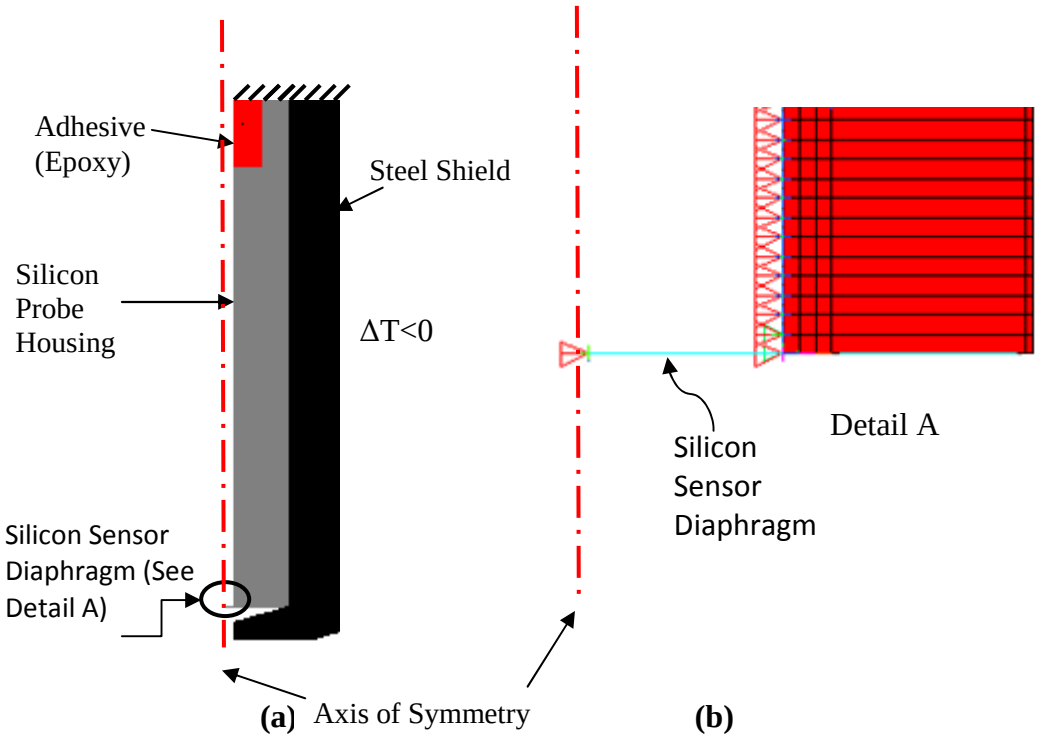

Fig. 2.2(a) Axisymmetric FEA model showing FOPS temperature loading and boundary conditions. Different materials are color-coded. (b) Detail A, a closer look at the meshed diaphragm

2.2.2 Material Properties

The FOPS consists of three different materials. The outer shield, which encompasses the probe housing, is made from steel. The probe housing and the diaphragm are

made of silicon material. The material properties are listed in the Table 2.1 below and the different material locations are illustrated in Fig. 2.2(a) with different colors.

Table2.1. List of material properties used in the FEA model

	Steel (Shield)	Silicon (Probe Housing and Diaphragm)	Adhesive
Density (kg/m^3)	7820	2330	1720
Poisson's ratio	0.27	0.28	0.28
Young's modulus (GPa)	200	112.4 - 165	2.26
Coefficient of thermal expansion (K^{-1})	15.2E-6	3.2E-6	191E-6

2.3 FEA Model Validation

The FEA model development for the FOPS is guided by a simplified preliminary linear analytic model of a simple pressure loaded plate. Bending of the thin circular diaphragm in the FOPS can be simply modeled as a thin circular elastic plate with uniform transverse pressure loading. The finite element solution for this simplified

problem can be compared to the known elastic solution given by Timoshenko [9]. The plate is made of silicon with Young's modulus 112.4 GPa and Poisson's ratio of 0.28. The radius of the disk is 50μm and the thickness is 5μm. The plate is clamped at the boundary and is loaded with a uniform pressure load *p* (=1.0 bar), as shown in Fig. 2.3. Since the thickness to diameter ratio is low (0.05), we use Kirchhoff's plate formulation for the analytic solution.

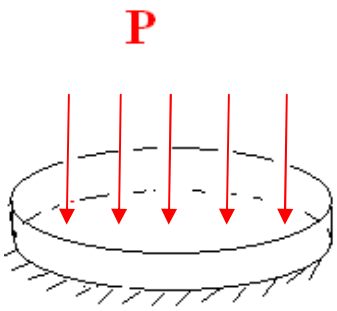

Fig. 2.3. Clamped Circular plate with uniform pressure loading, P

2.3.1 Analytic solution (Kirchhoff Plate Formulation)

The maximum displacement and the maximum stress of the diaphragm using Kirchhoff approach for a plate is expressed as [9]:

$$w_{max} = \frac{Pr^4}{64D}, \tag{2.1}$$

$$\sigma_{max} = \frac{3Pr^2}{4t^2} \tag{2.2}$$

where w_{max} is the displacement, σ_{max} is the max stress, *P* is the pressure; *r* is the radius of the disk, t is the plate thickness and *D*, the flexural rigidity, is given by [9]:

$$D = \frac{Et^3}{12(1-v^2)}, \tag{2.3}$$

where E is the Young's modulus, t is the thickness and v is the Poisson's ratio.

Substituting numerical values of our case: E= 112.4 GPa, p=1bar, r= 50μm, v= 0.28 and t= 5μm, we obtain the deflection to be 7.7nm and stress to be 7.9 MPa.

2.3.2 FEA Model

The circular silicon diaphragm presented in Sec. 3.1 is modeled with an axisymmetric shell element with a user defined thickness. The axis-symmetric FEA model of the thin plate, meshed with 10 elements, is shown in Fig. 2.4. The model is constrained in the axial and the radial direction at its circumperence and the rotation is also set to zero there. At its center, the diaphragm is free to move in the axial direction but is constrained in the radial direction and the rotation is also set to zero here. Symmetry boudary condition is also applied to the center of the diaphragm. And the material and geometry properties of E= 112.4 GPa, r= 50μm, v= 0.28 and t= 5μm were input just as they were for the analytic model.

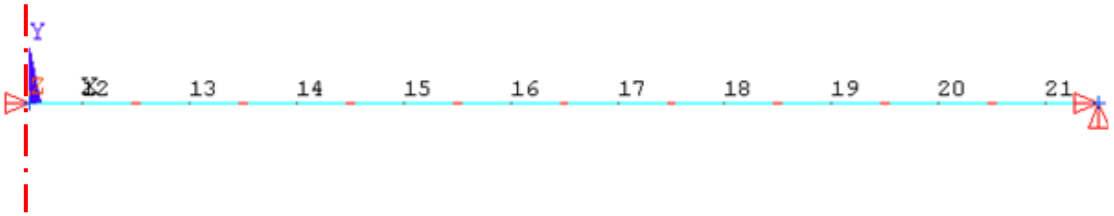

Fig. 2.4. Meshed axisymmetric model

Under the pressure load of p=1bar, the max deflection at the diaphragm center, obtained from FEA solution, is 8.0nm for 1 bar pressure and the max stress at the diaphragm edge is 6.4 MPa. The solution obtained from the FEA model matches the

analytic solution based on Kirchhoff approach, given in Sec. 3.1, within 4%. The FEA solution is a bit higher due to the fact that Kirchhoff's approach assumes the diaphragm as a plate, and ignores the additional compliance due to membrane stretching and transverse shear deformations, both of which are included in the FEA shell element chosen in this study. This error is considered acceptable and the number of elements of the diaphragm is fixed at 10 for this part of the study. In the FEA model of the entire sensor assembly, the absolute displacement of the diaphragm is expected to be larger than the value estimated above, because the probe housing also deforms under external pressure. However, the displacement of the diaphragm's center point relative to its circumference is expected to be very close to the analytic and FEA solutions of the simple clamped diaphragm presented earlier.

2.4 Parametric Results of FOPS Linear FEA Model

As mentioned above, the item of interest is the sensor diaphragm shown in Fig. 2.1. The diaphragm nominal dimensions are 100μm diameter and 5μm thickness. When subjected to 1.0 bar pressure, as shown in Fig. 2.2(a), the resulting maximum deflection is 9.1nm at the geometric center of the diaphragm, as shown in Fig. 2.5(a). The deflection is higher than either the analytic solution or the FEA model of a simple clamped shell, due to the fact that the periphery of the diaphragm is no longer constrained in the axial direction. The diaphragm will experience an axial deflection at the center as well as the periphery which is found to be 1.1 nm. The corresponding maximum principal stress due to diaphragm bending is 6.9 MPa and it occurs near the diaphragm periphery at the bottom surface, as shown in Fig. 2.5(b).

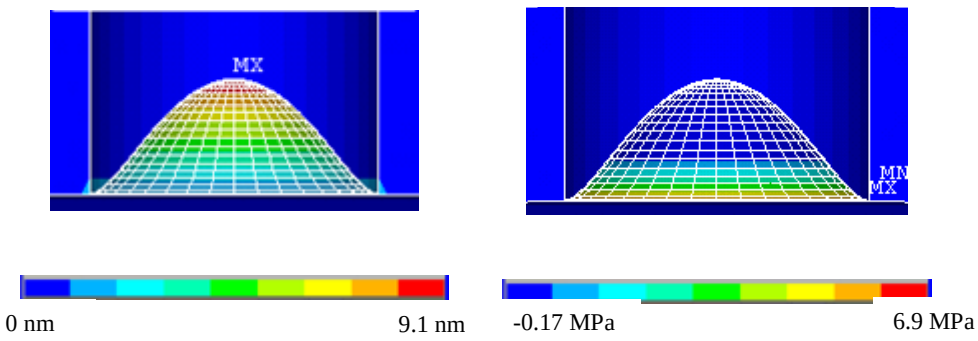

(a) **(b)**

Fig. 2.5. (a) Deflection of the sensor diaphragm under pressure loading of 1.0 bar (magnified 5K times) and (b) principal stresses in the diaphragm

2.5 Design Investigations for Diaphragm Thickness

Once the 5μm thick Silicon diaphragm was analyzed under the working loading condition of 1.0 bar pressure, the thickness of the diaphragm was varied between 1μm and 5μm to study its effect in the linearized FEA model, on the sensitivity and on the stress margins in the diaphragm based on fracture.

2.5.1 Linearized Stress Margins: Diaphragm Fracture

The maximum stress in the diaphragm obtained from FEA simulations are compared against silicon fracture strength, which is fixed here at 7000 MPa [17]. The predicted maximum principal stress (6.9 MPa), due to 1.0 bar pressure loading, is clearly much

less than the fracture strength (7000 MPa) of the diaphragm material. The increase of the stress in the diaphragm with decreasing thickness is shown in Fig. 2.6. This figure demonstrates the linearized FEA prediction of the relationship between the stress ratio (max principal stress/fracture strength) and the maximum deflection of the diaphragm, with changing diaphragm thickness, for a unit loading of 1.0 bar. As the diaphragm thickness is reduced from 5 µm to 1 µm, the diaphragm sensitivity increases by two orders of magnitude and the stress ratio increases by an order of magnitude itself. We can see from Fig. 2.6 that at thickness of 5µm, there is a substantial design margin with respect to the stresses in the diaphragm and that the diaphragm thickness can be reduced to increase the sensitivity without risking fracture of the diaphragm.

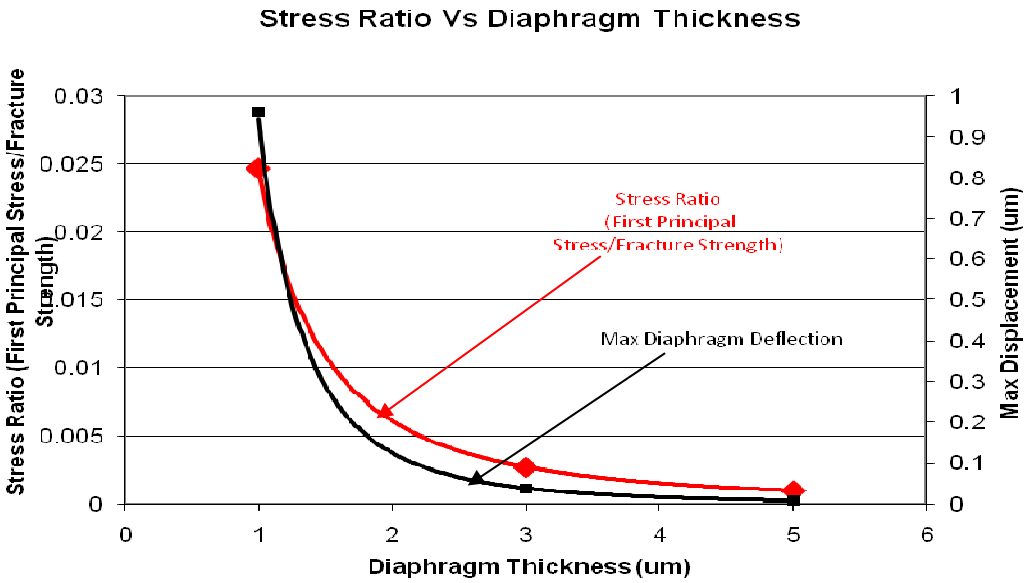

Fig. 2.6. Comparison of stress ratio (principal stress/fracture strength) and max deflection of the diaphragm with changing diaphragm thickness

While the sensitivity varies inversely with the diaphragm thickness, the stress margin increases as the thickness increases. Fig. 2.7 summarizes these results. In this figure, two normalized indices are introduced; namely, (1) normalized diaphragm sensitivity, which is the ratio of the diaphragm maximum displacement (measured at 1.0 bar) to diaphragm thickness and (2) pressure loading safety factor, which is the ratio of Silicon fracture strength (measured at 1.0 bar pressure) to the maximum first principal stress in the diaphragm. These graphs clearly illustrate the competing trade-offs between design sensitivity and design margins. To find the absolute sensitivity and design margins, the results should be scaled by the magnitude of the pressure change.

Clearly this simplified linearized result cannot be used beyond pressures that cause deflection in excess of about 30% of the thickness of the plate, since nonlinear effects can no longer be ignored beyond this deflection magnitude. As an example, this linear analysis is not accurate enough for results at 10 bar pressure, for any diaphragm thicknesses below about 1.25μm, where the diaphragm sensitivity ratio will reach an approximate value of 0.30. Similarly at 10.0 bar pressure, linearized results are valid only for $t > 2.5\mu m$. For more detailed assessment, nonlinear analysis is needed, as discussed in Sec. 2.6.

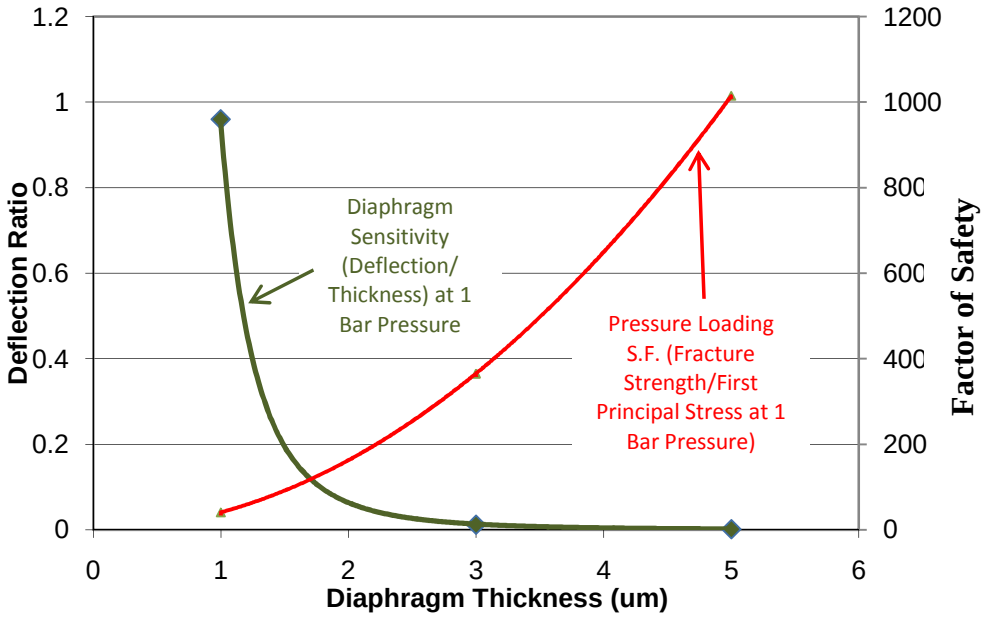

Fig. 2.7 Trade-off between diaphragm sensitivity and stress margin for fracture

2.6 Nonlinear Diaphragm Deflection Analysis

As discussed in Sec. 2.5, the linearized results obtained in the analyses are no longer valid when the deflection of the diaphragm approaches 30% of its thickness. Nonlinear effects limit the measurement range of the sensor and have to be taken into consideration. Additional research has been conducted to include geometric nonlinearity in the finite element analysis of the sensor diaphragm. Fig. 2.8 shows the nonlinear deflection of diaphragm of different thicknesses in response to different pressure levels. For a diaphragm of 5μm thickness, the response is linear upto the 100.0 bar pressure loading and for a 1μm thick diaphragm the response is nonlinear even at 1.0 bar pressure loading. As the diaphragm thickness decreases, nonlinearity

of the response becomes increasingly severe and must be taken into account for assessing the FOPS sensitivity and stress margins.

As discussed in Sec 2.5, the diaphragm thickness has to be optimized to satisfy competing design constraints of maximizing the sensitivity and minimizing the stresses causes by pressure changes. Nonlinear analysis of deflection and stresses due to pressure loading are discussed here. Fig. 2.9 illustrates the stress ratio (max principal stress/fracture strength) in the diaphragm for different diaphragm thicknesses and different pressure levels. As the diaphragm thickness is reduced the sensitivity as well as the stress in the diaphragm increase. We can see from Fig. 2.9 that there is a substantial design margin with respect to the stresses in the diaphragm as the stress ratio is below unity. The diaphragm thickness can be reduced to increase the sensitivity and still keep the stresses much below the fracture strength. This implies that the failure of diaphragm due to overstress will not be a governing factor over the deflection of the diaphragm as the diaphragm response will become nonlinear well before the stresses become significant.

The diaphragm responds linearly in a certain pressure range, depending on the thickness. This linear range indicates the working range of the FOPS. The error criterion used in this study for defining the linear operating range is 3% deviation from linear response. This criterion is very similar to error levels used in the industry [10]. Fig. 2.10 shows the percent error obtained as the diaphragm thickness and the pressure loadings are varied. Fig 2.10 shows that a sensor with a diaphragm thickness of 5μm is well within the working range upto 100 bar pressure. As the diaphragm

thickness is reduced, the 3% error occurs at lower pressures, therefore reducing the operating range of the sensor. Using Fig. 2.10, the sensor can be designed for a certain diaphragm thickness based on sensitivity and working pressure range. For example, a sensor with a diaphragm of 3μm thickness has a working range of 0 to 20.0 bar pressure loading.

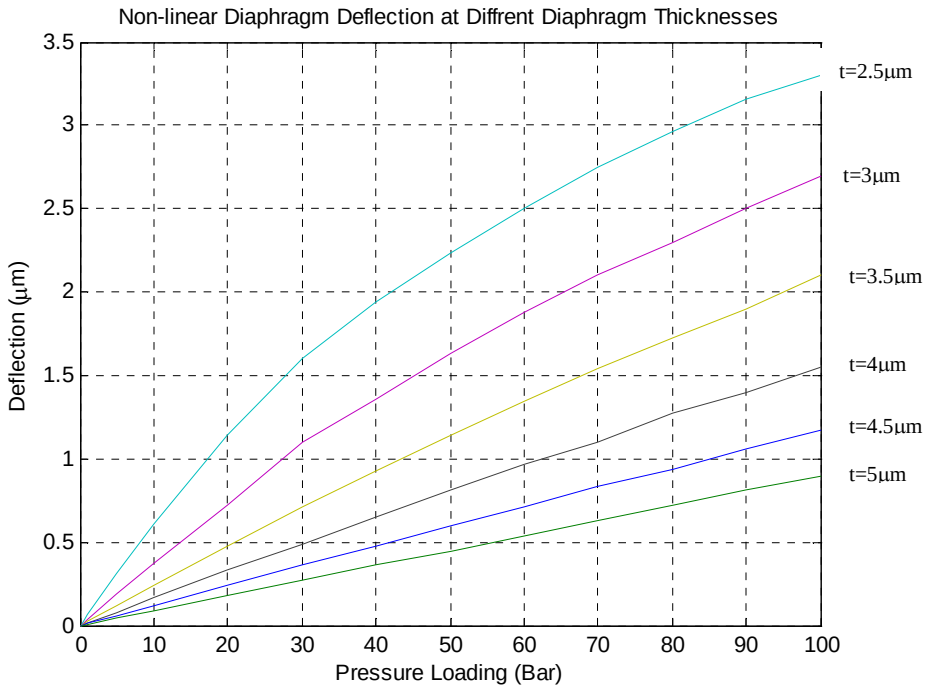

Fig. 2.8 Nonlinear diaphragm deflection at different diaphragm thicknesses

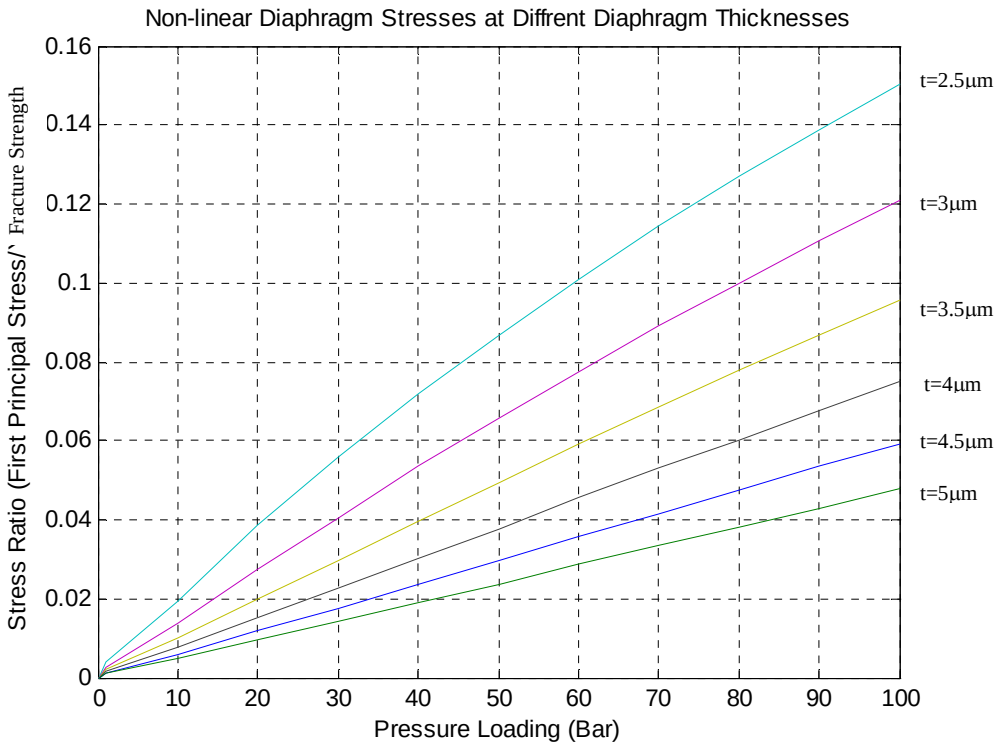

Fig. 2.9 Nonlinear diaphragm stress ratio (first principal stress/fracture strength) of different diaphragm thicknesses with increasing pressure loading

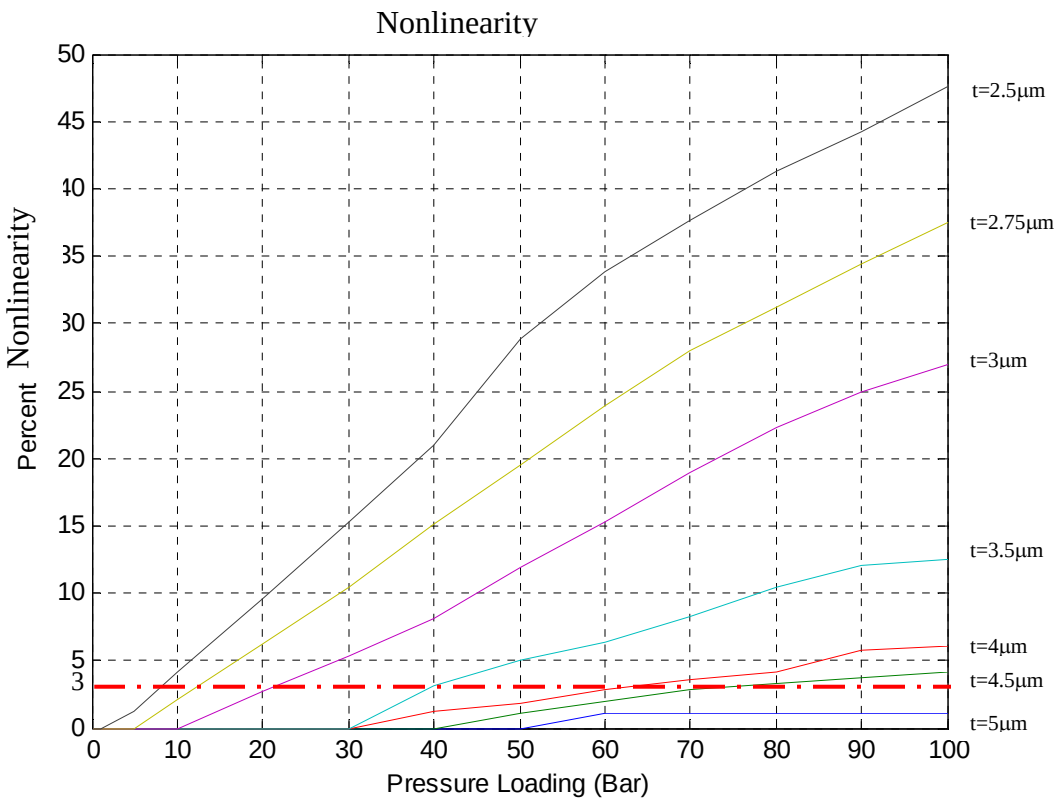

Fig. 2.10. Deviation from linearity in diaphragm response for different thicknesses and pressures

Fig. 2.11 shows a contour plot of the normalized diaphragm deflection (deflection/thickness) and the nonlinearity in the diaphragm response with changing diaphragm thickness and pressure loading. Using Fig. 2.11, linear operating ranges can be defined using different nonlinearity criteria such as 1% nonlinearity up to 3% nonlinearity. For example, a 3 µm thick diaphragm in this FOPS design can be used upto 20 bar pressure if we accept upto 3% nonlinearity.

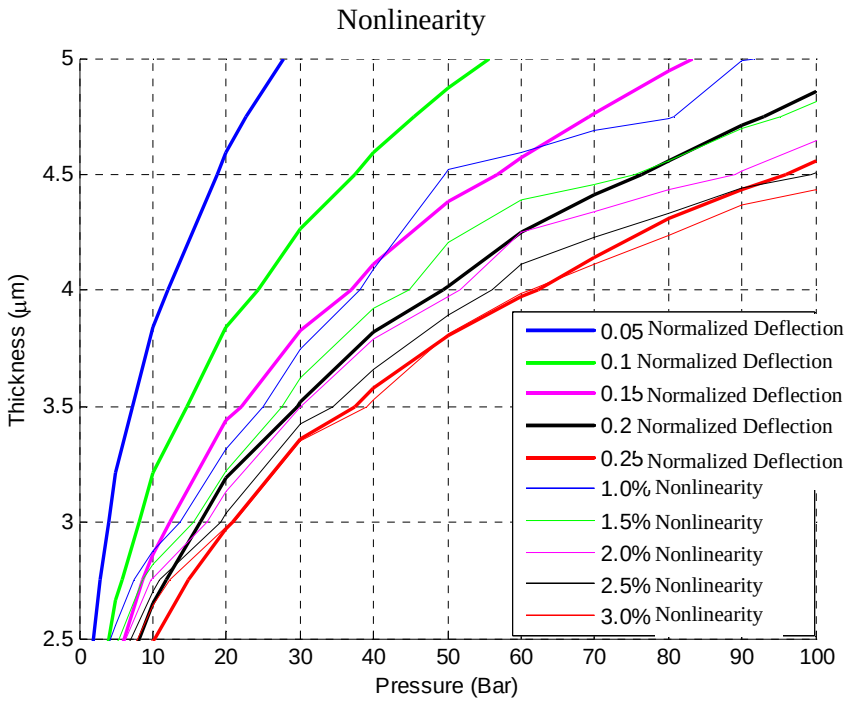

Fig. 2.11. Contour plot of the diaphragm deflection ratio (diaphragm deflection/diaphragm thickness) and the percent error of the difference of the linear and the nonlinear diaphragm deflection

2.7 Conclusions

In this study, the design trade-offs of the diaphragm of a fiber optic pressure sensor under field operating conditions is investigated. The field operating conditions are defined in terms of external pressure. The work conducted shows that the reliability is not a problem for any practical pressure range. As it was noted from Fig. 2.9, the stresses in the diaphragm are much below the fracture strength of silicon for even small thicknesses. However, diaphragm deflection nonlinearity plays a vital role in the design and limits the operating range of the diaphragm as illustrated in Fig. 2.10.

Thus there are conflicting design criteria and results have been presented to allow designers to trade off the measurement sensitivity vs the operating range, using different nonlinearity criteria from 1-3%.

2.8 Acknowledgements

This research is funded in part by Pervasive Technology Engineering, LLC and in part by the State of Maryland through MIPS contract # 3837. The authors thank Dr. M. Eltoweissy from the company for providing technical assistance needed for the project.

2.9 References

[1] Shilpak, M., Dugundji, J., "Large deflections of clamped circular plates under initial tension and translation of membrane behavior," ASME Journal of Applied Mechanics Papers 65, 107-115 (1998)

[2] Yu, M., Balachandran, B., "Sensor diaphragm under initial tension: linear analysis," Experimental Mechanics Papers 45, 123-129 (2005)

[3] Zheng, N., Shi, C., Wang, D., Zhang, M., Liao, Y., "Diaphragm type fiber optic interferometric acoustic sensors, Optical Engineering," Papers 42, 2558-2562 (2003)

[4] Yu, M., Balachandran, B., “Acoustic measurements using fiber optic sensor system,” Journal of Intelligent Material Systems and Structures Papers 14, 409-414 (2003)

[5] Yu, M., Long, X., Balachandran, B., “Sensor diaphragm under initial tension: nonlinear responses and design implications,” Journal of Sound and Vibration Papers 312, 39-54(2005)

[6] Al-Bassyiouni, M., Yu, M., Balachandran, B., Oh, J., “Fiber optic sensors for active acoustic control,”Proc. SPIE 4693, 39-54 (2005)

[7] Soedel, W., [Vibrations of shells and plates], Marcel Dekker, New York, 1993

[8] Kalamkarov, A., MacDonald, D., Fitzgerald, S., Georgiades, A., “Reliability assessment of pultred FRP reinforcements with embedded fiber optic,” Composite Structures Paper 50, 69-78 (2000)

[9] Timoshenko, S., [Strength of Materials], Krieger Pub Co , 1976,

[10] PCB Piezotronics Inc. ICP Pressure Sensor Product Manual “http://www.pcb.com/contentstore/docs/PCB_Corporate/Pressure/products/Manuals/101A.pdf”

Chapter 3: Design Study of Fiber Optic Pressure Sensors at Different Operating Temperatures

The text of this chapter is taken from a paper that has been submitted for publication. This Chapter investigates the design constrains due to structural failure mechanism in the sensor and explores the design space by parametric design sensitivity study.

The rest of this document is organized as follows. A linear analytic solution for thermo-mechanical buckling of circular plates is discussed in Section 3.2. The FEA model for nonlinear analysis of thermo-mechanical stresses in the FOPS diaphragm is described in Section 3.3, and the results for thermo-mechanical stresses in the FOPS diaphragm are presented in Section 3.4. Nonlinear FEA prediction of buckling strength of circular clamped plates for different thicknesses is discussed in Section 3.5 and a parametric methodology for developing design guidelines is presented in Section 3.6, followed by conclusions in Section 3.7.

Design Study of Fiber Optic Pressure Sensors at Different Operating Temperatures

Yasir Majeed[1,*], Moustafa Al-Bassyiouni[1], Abhijit Dasgupta[1]

[1]Department of Mechanical Engineering, University of Maryland, College Park, MD 20742, USA

[*]Corresponding author: ymajeed@umd.edu

Abstract

This paper parametrically explores the nonlinear buckling strength and post-buckling deformations of the diaphragm of a fiber optic pressure sensor (FOPS), due to the generation of thermo-mechanical radial stresses caused by drop in the application temperature. The product under study is a miniature FOPS that can be embedded in, or installed on, a structure for pressure monitoring applications. The field operating conditions are defined in terms of temperature and pressure. The FOPS probe has a Fabry-Perot cavity, with the fiber tip and a miniature diaphragm acting as the two mirrors. The cavity length changes when the diaphragm deflects under pressure. However, due to field operating conditions, thermal and pressure loads can generate failure mechanisms such as buckling of the diaphragm and limit the structural and optical operating limits of the sensor. With the aid of nonlinear thermo-mechanical finite element analysis, this study investigates design constraints due to nonlinearities and structural failure mechanisms in the sensor and explores the design space by a parametric design sensitivity study. A methodology is illustrated to allow the

designer to trade-off sensitivity vs the operating temperature and pressure range of a selected FOPS design.

Keywords: Fiber-optic pressure sensor; Fabry-Perot interferometer; nonlinear finite element analysis, thermo-mechanical stress diaphragm buckling, parametric design optimization

3.1 Introduction

Diaphragms are commonly used in sensors for dynamic pressure sensing, where the dynamic pressure is detected through the deflection of the diaphragm. In this study, the diaphragm displacement is detected with a fiber optic sensing circuit. Fiber Optic Pressure Sensors (FOPS) have the advantage of being light weight and having high sensitivity. The sensing is based on detecting the optical phase change induced by the change in the optical path length as the diaphragm deflects under a pressure loading. The FOPS probe has a Fabry-Perot cavity with the fiber tip and a miniature diaphragm acting as the two mirrors, where the cavity length changes when the diaphragm deflects under pressure. However, due to field operating conditions, the diaphragm deflection can be in part due to diaphragm buckling under thermo-mechanical loading, thus compromising the accuracy of the pressure measurement. Sources of failure in our study are in the diaphragm due to temperature and pressure. Additional errors may occur due to fiber expansion, changes in refractive index and changes in air properties, but are not considered in this study.

Because the sensitivity of the sensor is related to the behavior of the thin diaphragm, choosing a suitable diaphragm design is important for optimizing the sensor parameters. Diaphragm thickness is an important factor in the sensitivity of the sensor. As the diaphragm thickness is reduced, the sensitivity increases but at the expense of increasing the stresses and fatigue damage in the diaphragm and also reducing its buckling strength. The design has to be optimized based on trade-offs between sensitivity and buckling margins. To conduct the optimization, models must be developed that quantify the sensitivity of the sensor and the reliability margins, under pressure and thermal loading. With the aid of finite element analysis, this study investigates the reliability of fiber optic sensor diaphragm under temperature and pressure loadings and its influence on the design optimization of the diaphragm.

Studies have been reported in the literature to optimize FOPS diaphragm sensitivity. Shilpak and Dugungi [1] conducted static analyses of a clamped circular plate under initial tension and studied the plate behavior and when the plate transitions into a thin membrane/diaphragm in terms of a non-dimensional tension parameter k which is proportional to the square-root of the tension loading and the radius of the clamped plate, and inversely proportional to the bending stiffness of the clamped plate. This transaction occurs over the range $1<k<20$. The behavior is that of a thin plate for $k<1$, and like a thin membrane when $k>20$. Yu and Balachandran [2] studied the diaphragm response in terms of this tension parameter k and showed that the analysis and the results can be used to design a sensor diaphragm to maximize sensitivity. In

recent work [3-5] there has been emphasis on optimization of the sensitivity of the sensors by studying the diaphragm deflection.

If the diaphragm experiences compressive in-plane stresses due to thermo-mechanical constraints from the sensor housing, the sensor may become unstable and out-of-plane buckling may occur without any other external forces being present [7]. This phenomenon is known as thermal buckling, and the temperature corresponding to the critical load is called the buckling temperature [8]. Beyond this critical load, deformations are not proportional to the applied pressure, thus compromising the pressure measurement capability of the sensor. Furthermore, the large buckling-induced deformations may become considerable and may rupture the diaphragm [7]. In the previous work of Majeed et. al. [9], design margins were investigated not only for the sensitivity of the thin diaphragm but also for the stresses developed in the diaphragm, which are critical to failure. Design trade-offs were demonstrated for the same FOPS, with respect to sensor sensitivity, sensor operating range and fracture due to excessive stresses on the diaphragm. Majeed et. al. [1] put forth design margins for the optimal design of the FOPS diaphragm under external pressure loading only. In reality, the FOPS will not only be exposed to a changing pressure environment, but also to varying operating temperatures. The additional effects due to temperature changes are examined in this study.

The internal construction of the fiber optic pressure sensor, FOPS, under study is shown in Fig. 3.1 (a). The point of interest in this model is the thin diaphragm circled. The FOPS must withstand environmental temperature changes in operation. When

the temperature drops, the outer steel shield will shrink more than the inner silicon probe housing and the thin silicon diaphragm. The resulting compressive radial stress in the diaphragm may cause the diaphragm to buckle as the thickness is reduced for better sensitivity. Thus the diaphragm thickness must be optimized to minimize the risk of buckling. This paper will investigate the design margins of the FOPS due to the buckling of the diaphragm.

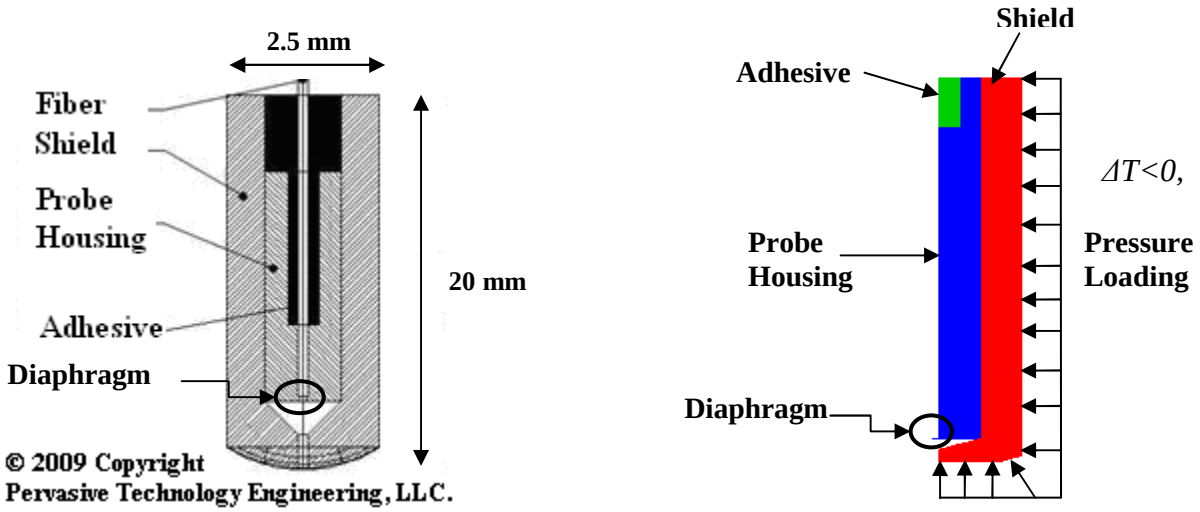

Fig. 3. 1 (a) Internal construction of the fiber optic pressure sensor (FOPS) (b) Thermal and pressure loading on the FOPS

The rest of this document is organized as follows. A linear analytic solution for thermo-mechanical buckling of circular plates is discussed in Section 3.2. The FEA model for nonlinear analysis of thermomechanical stresses in the FOPS diaphragm is described in Section 3.3, and the results for thermomechanical stresses in the FOPS diaphragm are presented in Section 3.4. Nonlinear FEA prediction of

buckling strength of circular clamped plates for different thicknesses is discussed in Section 3.5 and a parametric methodology for developing design guidelines is presented in Section 3.6, followed by conclusions in Section 3.7.

3.2 Thermomechanical Buckling: Analytic Solution

The diaphragm, which can be assumed to be a thin circular plate with clamped edges, is placed under radial compressive stress, as shown in Fig. 3.2. The in-plane compressive radial stresses are generated by the CTE mismatch during cool-down. The diaphragm buckles when the in-plane compressive stress exceeds a critical threshold.

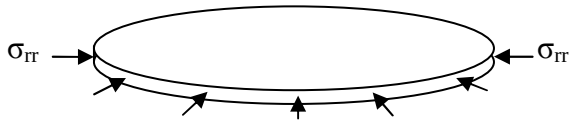

Fig. 3.2. Circular Diaphragm under radial stress

The critical buckling strength of a plate, λ_{cr}, is obtained by the relation [7]

$$\lambda_{cr} = \frac{-14.68Et^2}{12r^2(1-v^2)} \quad , \tag{3.1}$$

where E is the elastic modulus, t is the thickness, r is the radius of the plate and v is the Poisson's ratio. Theoretically, this means that for a Si diaphragm with E=112.4 GPa, t=5 µm, r=50 µm, v=0.28, the required stress to buckle the diaphragm, λ_{cr}, is approximately 1.5 GPa.

The next step is to estimate the in-plane compressive stress generated by the temperature drop ΔT [7]:

$$\sigma_{rr} = \frac{-E\alpha\Delta T}{(1-\upsilon^2)}. \quad (2)$$

where α is the relative coefficient of thermal expansion between steel and silicon. As we see in Fig. 3.3, the stress ratio (radial stress/buckling strength) decreases as the diaphragm thickness increases and increases with the increase in temperature drop (ΔT). Here α=12E-6 /K

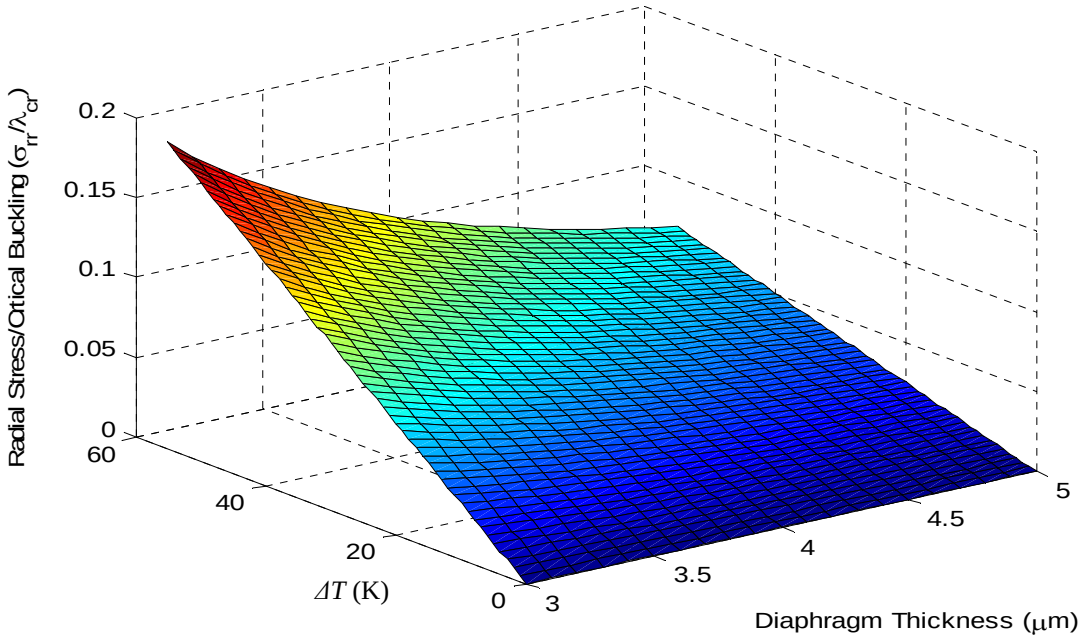

Fig. 3.3 Stress ratio (radial compressive stress / critical buckling stress) with varying ΔT and diaphragm thickness

3.3 FEA Model

The model for nonlinear finite element analysis (FEA) of the thermo-mechanical stresses in the FOPS is described in this section. The internal construction of the fiber optic pressure sensor under study is shown in Fig. 3.1(a). In light of the axisymmetric structure and loading a 2-D axis-symmetric finite element model is used, rather than a full 3-D model, to minimize calculation time. Details of the model are illustrated in Fig. 3.4. The point of interest in this model is the thin diaphragm circled in Fig. 3.1(a). In this study, there are two different types of axisymmetric elements used: (1) the diaphragm is modeled using 20 axisymmetric, 2-node, shell elements; (2) the rest of the FOPS body, which includes the shield, probe housing and the adhesive is modeled using 5,361 4-noded axisymetric brick elements. The rotation of the shell elements is constrained to the brick element. Fig. 3.4(a) shows the entire sensor under pressure loading and boundary conditions arrows indicate the thermal loading, hash markings indicate the kinematic boundary condition and different materials are assigned different colors for better visualization. Fig. 3.4(b) shows a closer view of the diaphragm. The sensor is subjected to a thermal loading of a drop in temperature, ΔT (Fig. 3.4(a)). This generates compressive radial forces on the sensor diaphragm due to the coefficient of thermal expansion (CTE) mismatch between the steel housing and the silicon sensor element. The top is constrained in all three degrees-of-freedom (Fig. 3.4(a)). Symmetry condition is applied along the axis of symmetry along the axial direction.

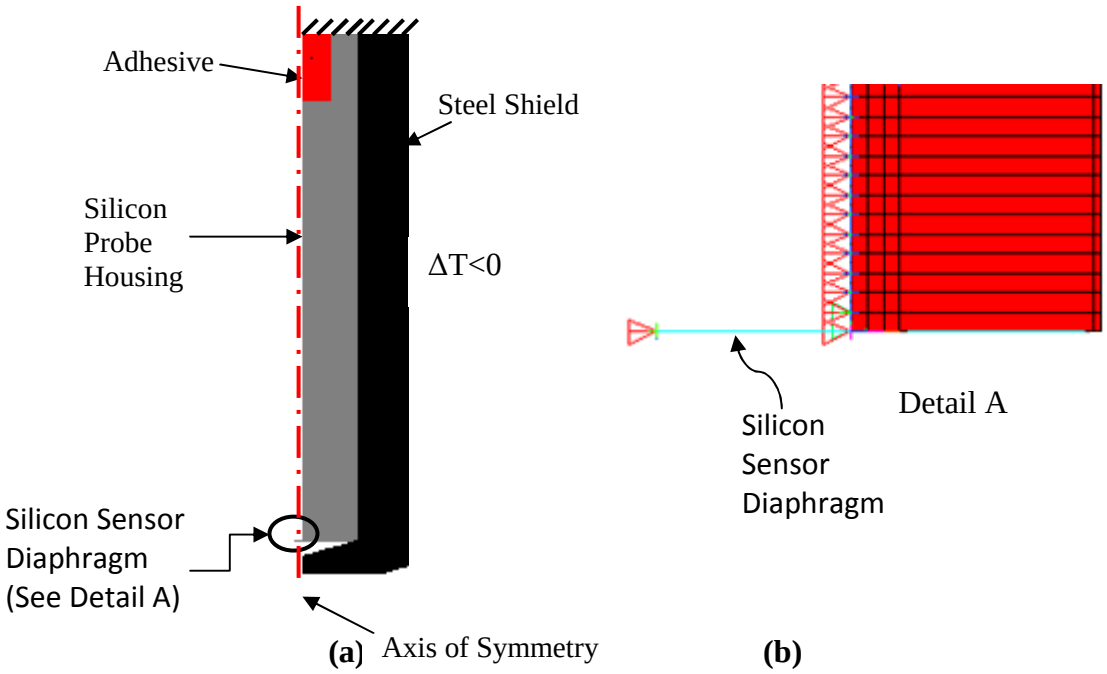

Fig. 3.4(a) Axisymmetric FEA model showing FOPS temperature loading and boundary condition. Different materials are color-coded. (b) Detail A, a closer look at the meshed diaphragm

The FOPS consists of three different materials. The outer shield, which encompasses the probe housing, is made from steel. The probe housing and the diaphragm are made of silicon material and the adhesive encompasses the fiber. The material properties are listed in the Table 3.1 below.

Table 3.1. List of material properties used in the FEA model

	Steel (Shield)	Silicon (Probe Housing and Diaphragm)	Adhesive
Density (kg/m^3)	7820	2330	1720
Poisson's ratio	0.27	0.28	0.28
Young's modulus (GPa)	200	112.4 - 165	2.26
Coefficient of thermal expansion (K^{-1})	15.2E-6	3.2E-6	191E-6

3.4 Nonlinear Parametric FEA Prediction of Thermo-mechanical Stresses in FOPS Diaphragm

As mentioned above, the structure of interest is the 100μm diameter diaphragm of the FOPS shown in Fig. 3.1(a). The FEA results are presented for parametric variation of the diaphragm thickness from 1 μm to 5 μm, and for parametric temperature drop between 0 and -150 °C. Figure 3.5 shows the in-plane compressive radial stresses generated in the analyzed cases. The stresses have been normalized, for convenience, by the buckling strengths estimated for each thickness from the simple analytic model of a clamped circular plate in Equation 3.1.

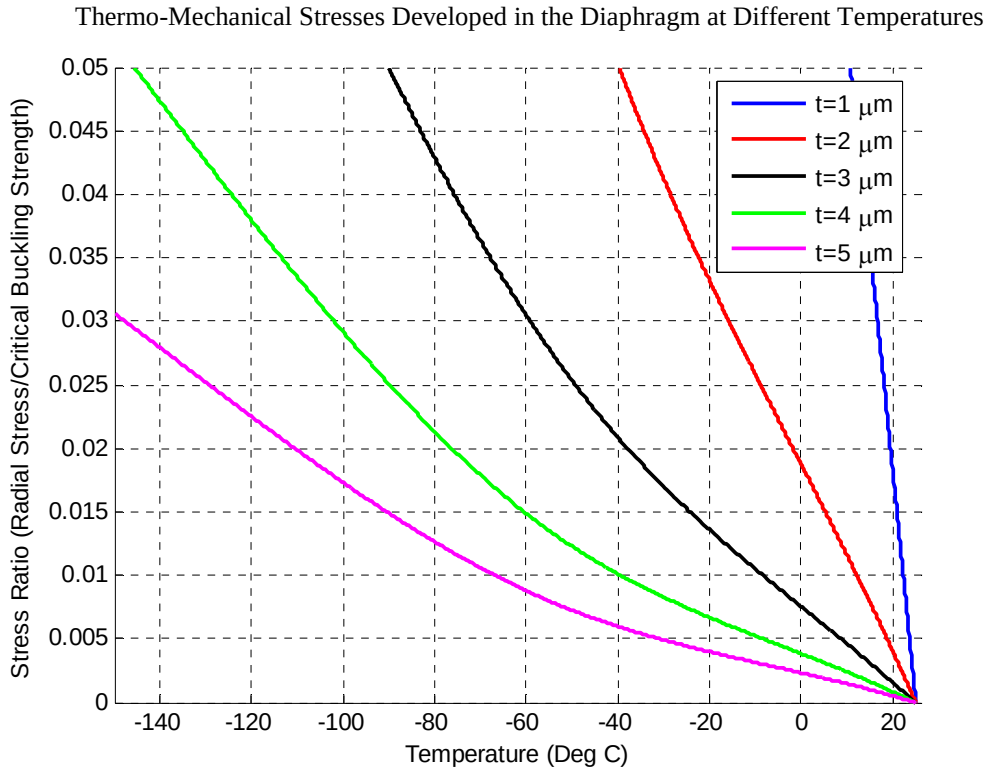

Figure 3.5 Parametric Results of Thermo-mechanical Stresses in FOPS Diaphragms of Different Thicknesses Due to Temperature Drop of Different Ranges

These stress results are used later in Sec. 3.5, for design of the FOPS thickness to maximize sensitivity without buckling under the operational FOPS temperature changes.

3.5 Nonlinear FEA Parametric Studies of Diaphragm Buckling Due to Temperature Change

Clamped circular plates with the dimensions and material properties described above for the FOPS diaphragm are modeled in finite element analysis (FEA) using commercial software. The accuracy of the FEA buckling strengths are compared with the analytic solution from Equation 3.1 in Sec 3.2.

The 3D diaphragm is modeled as an axisymmetric shell using 20 axisymmetric shell elements with user-defined thickness. The number of elements was chosen after preliminary trials, by matching the FEA buckling strength with the analytic predictions from Section 3.2. The meshed axisymmetric FEA model of the thin circular clamped is shown in Fig. 3.6. The diaphragm, now only a two-dimensional line, is placed under a radial stress and boundary and loading conditions are also illustrated in Fig. 3.6 The shell elements were constrained from rotation at the periphery and the axial center of the diaphragm**.** As is typical in buckling studies, a small transverse load, 0.005% of the applied compressive radial stress, is applied to the center of the diaphragm, to facilitate buckling. The buckling strength is parametrically investigated for different diaphragm thicknesses from 1 to 5 µm.

The diaphragm buckling curves for these cases is shown in Fig. 3.7. The radial stress at which the diaphragm buckles reduces as the diaphragm thickness is reduced, from 1.5 GPa for 5μm thickness to 60 MPa for a 1μm thickness

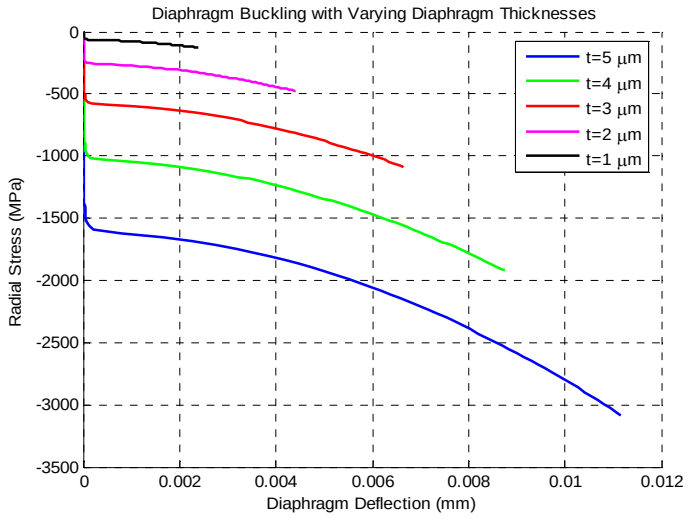

(a)

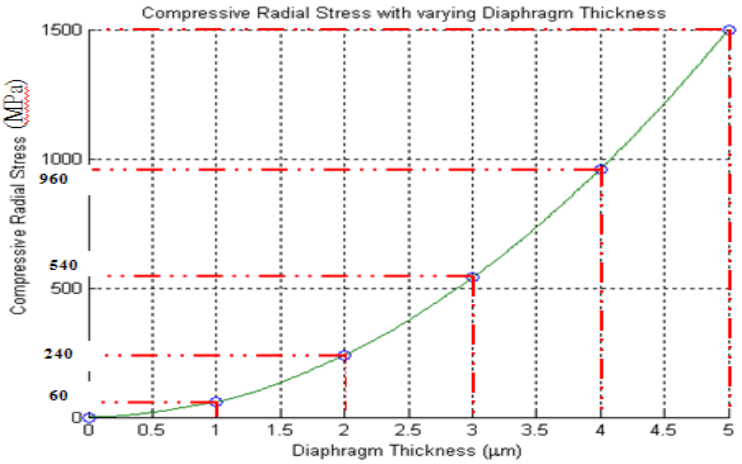

(b)

Fig. 3.7 (a) Diaphragm buckling strength of the FOPS as the diaphragm thickness is varied. (b) A closer look at the radial stresses at which the diaphragms buckle

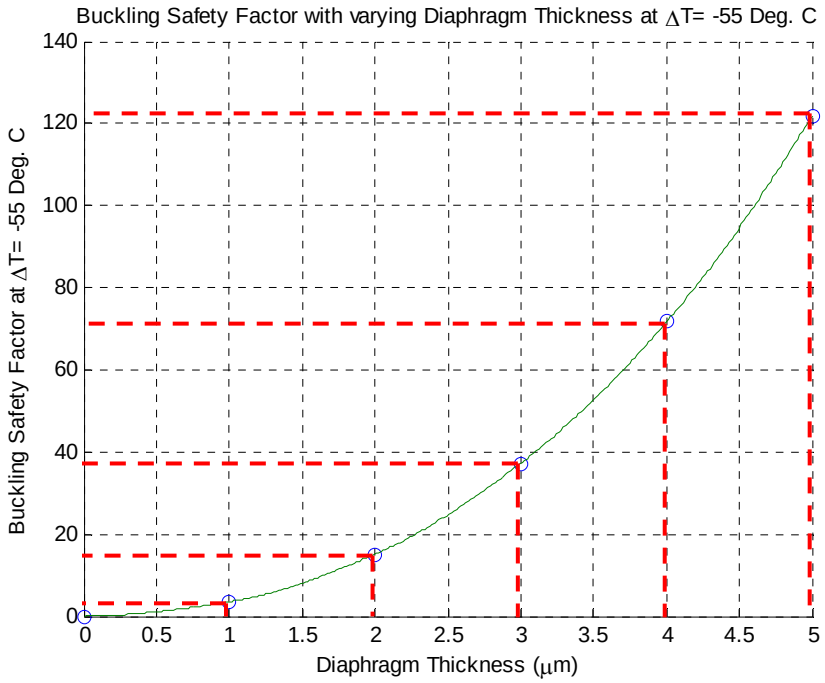

Fig. 3.8 Design margins for 100 µm silicon diaphragms of different thicknesses for temperature drop of -55 °C.

The buckling results in Figure 3.7 can be combined with the thermo-mechanical stress results of Figure 3.5, to estimate the buckling margins of safety for different temperature drops and for clamped circular diaphragms of 100 µm diameter and different thicknesses. As an example, Figure 3.8 shows the buckling design margins for temperature drop by -55°C, for diaphragms of 1-5 µm thicknesses. The in-plane radial stress is normalized by the corresponding buckling strength predicted by the linear analytic model of Section 3.2. It should be noted here that at higher thicknesses, there are huge design margins, and that they reduce with the diaphragm thickness. The FOPS can be optimized here to have the smallest thickness possible at

this temperature to enhance the sensor sensitivity yet also preventing buckling. But in reality, the FOPS will be under a coupled working environment of temperature and pressure [9]. Sec. 3.5 will take into consideration this coupled loading condition.

Figure 3.7(a) also shows the post-buckling deformations.

3. 6 Nonlinear FEA Parametric Studies of Diaphragm Buckling Due to Combined Temperature and Pressure Change

In Sections 3.5 and 3.6, the silicon diaphragm was placed under a loading condition that consisted of temperature drop. However, as described in the previous work of Majeed et. al. [9] in typical use conditions, the FOPS will experience pressure loading in the presence of such temperature change. Therefore this section explores the diaphragm deflections under different combinations of temperature drop and pressure loading. Section 3.6.1 analyzes nonlinear diaphragm deflections under simultaneous, proportional changes in temperature and pressure, for different proportionality ratios. This represents application conditions where the FOPS will experience simultaneous changes in temperature and pressure. Section 3.6.2 analyzes nonlinear diaphragm deflection under sequential changes, with various magnitudes of temperature drop followed by monotonic pressure loading. This represents application conditions where the FOPS will have to measure pressure at steady ambient temperatures that are below the stress-free temperature.

3.6.1. Simultaneous (Proportional) Changes in Temperature and Pressure

The pressure is increased by p bars as the thermo-mechanical in-plane compressive stress is proportionately increased to the linear analytic buckling limit of the diaphragm. This proportional loading is continued up to twice the buckling stress to examine the post-buckling deformations. Three different proportionality ratios are examined, with p = 0.46 bars, 4.6 bars and 46 bars.

Fig. 3.9 (a) shows the nonlinear diaphragm deflection curves for p=0.46 bars, for different diaphragm thicknesses. For comparison, the nonlinear deflections under pure in-plane loading without any transverse pressure (presented earlier in Figure 3.7a) are also superposed. As expected, the thicker diaphragms show very little additional deflection (and associated drop in buckling limit or linearity limit), while the thinner diaphragms show a significant change in deflection.

As explained in the introductory sections, the deflection of the diaphragm changes the cavity length of the FOPS which gives a reading for a pressure measurement. If the diaphragm deflects due to thermo-mechanical buckling, the sensor output will be contaminated as the buckling-induced deflection will add to the deflection due to the pressure loading and the sensor data recorded will lose its significance. Figure 3.9(a) shows the total deflection due to the combined loading A convenient way to isolate the deflections due to diaphragm buckling (due to a drop in temperature) from that due to the bending of the diaphragm (due to the pressure load), the diaphragm deflections from the coupled (temperature and pressure) loading were normalized by the deflection due to pressure loading. The in-plane compressive stresses were also

normalized by the theoretical buckling strength, for better comprehension. This normalized plot is shown in Fig. 3.9 (b).

Upon a closer look (Fig. 3.9 (c)), the diaphragm deflection ratio (deflection due to thermal pressure loading/deflection due to pressure loading) is seen to reach 1.03, (i.e. the buckling deflection is 3% of the pressure deflection) when the radial compressive stresses at the diaphragm circumference reaches approximately 3% of the critical buckling stress for all of the different cases of diaphragm thickness.

Similarly, the trend continues when the pressure loading rate is increased by factors of 10 and 100, relative to the rate of in-plane compressive stress increase. The nonlinear deflections progressively increase and the buckling limits progressively decrease, as the pressure loading rate increases, as shown in Figures 3.10 and 3.11. In Figure 3.10, the pressure loading rate p (relative to in-plane compression rate, as defined at the beginning of this section) is increased to 4.4 bars and in Fig 3.11, to 46 bars. Interestingly, regardless of the magnitude of the pressure loading rate p and the diaphragm thickness, the normalized diaphragm deflection ratio (deflection due to combined thermo-mechanical and pressure loading, normalized by the deflection due to pure pressure loading) continues to reach 1.03 when the in-plane radial compressive stresses at the diaphragm circumference reach approximately 3% of the theoretical linear buckling strength predicted by Eq. 3.1.

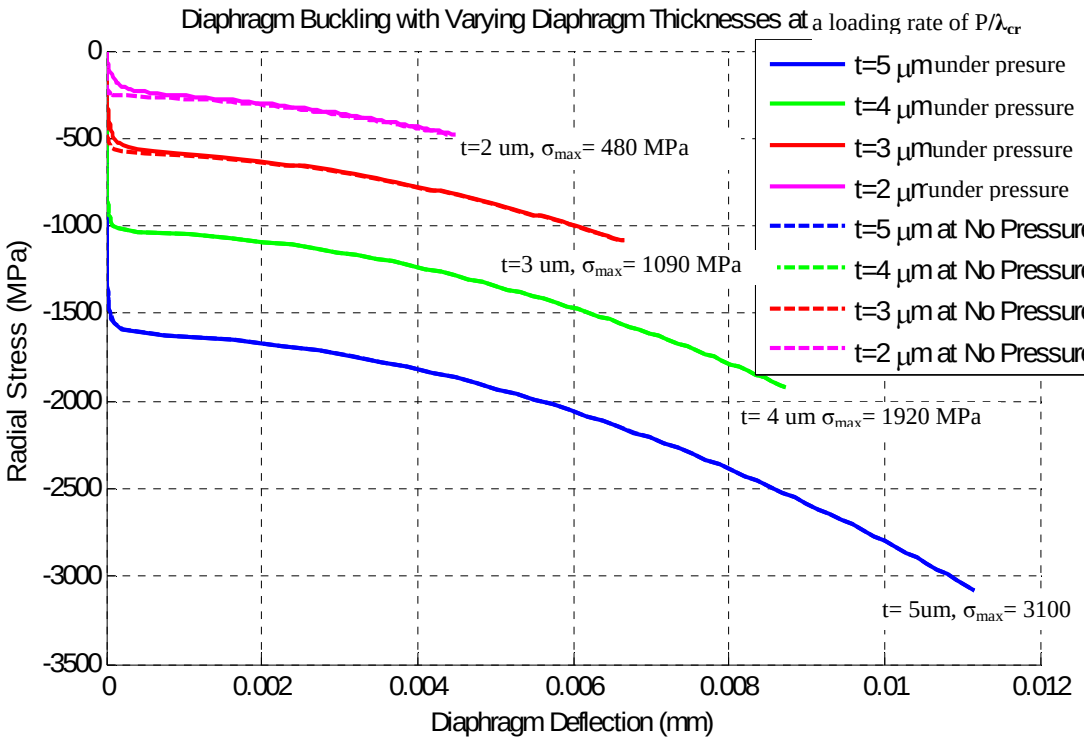
Diaphragm Buckling with Varying Diaphragm Thicknesses at a loading rate of P/λcr
Radial Stress (MPa)
Diaphragm Deflection (mm)
t=5 μm under presure
t=4 μm under pressure
t=3 μm under pressure
t=2 μm under pressure
t=5 μm at No Pressur
t=4 μm at No Pressur
t=3 μm at No Pressur
t=2 μm at No Pressur
t=2 um, σmax= 480 MPa
t=3 um, σmax= 1090 MPa
t= 4 um σmax= 1920 MPa
t= 5um, σmax= 3100
0
-500
-1000
-1500
-2000
-2500
-3000
-3500
0
0.002
0.004
0.006
0.008
0.01
0.012

(a)

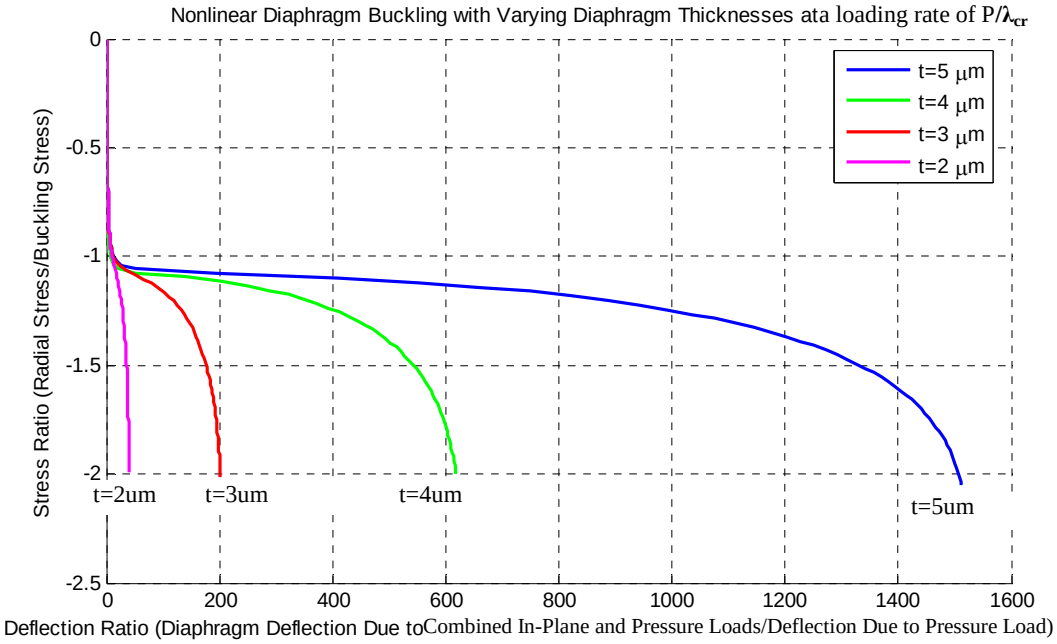
Nonlinear Diaphragm Buckling with Varying Diaphragm Thicknesses ata loading rate of P/λcr
Stress Ratio (Radial Stress/Buckling Stress)
Deflection Ratio (Diaphragm Deflection Due to Combined In-Plane and Pressure Loads/Deflection Due to Pressure Load)
t=5 μm
t=4 μm
t=3 μm
t=2 μm
t=2um
t=3um
t=4um
t=5um
0
-0.5
-1
-1.5
-2
-2.5
0
200
400
600
800
1000
1200
1400
1600

(b)

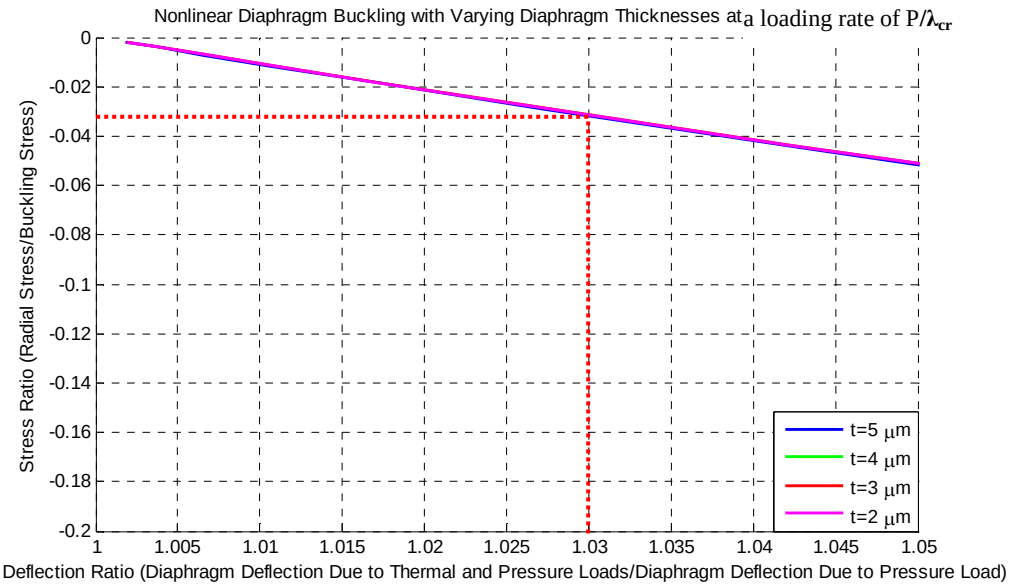

(c)

Fig. 3.9 (a) Nonlinear diaphragm deflection for p=0.46 bars increase of pressure, with proportional increase of in-plane compressive thermo-mechanical stresses up to the linear analytic buckling limit; for varying thicknesses, showing the nonlinearity before and after buckling. (b) Normalized diaphragm deflection curves. (c) A closer look at the normalized deflection curve showing the 'contamination limit'.

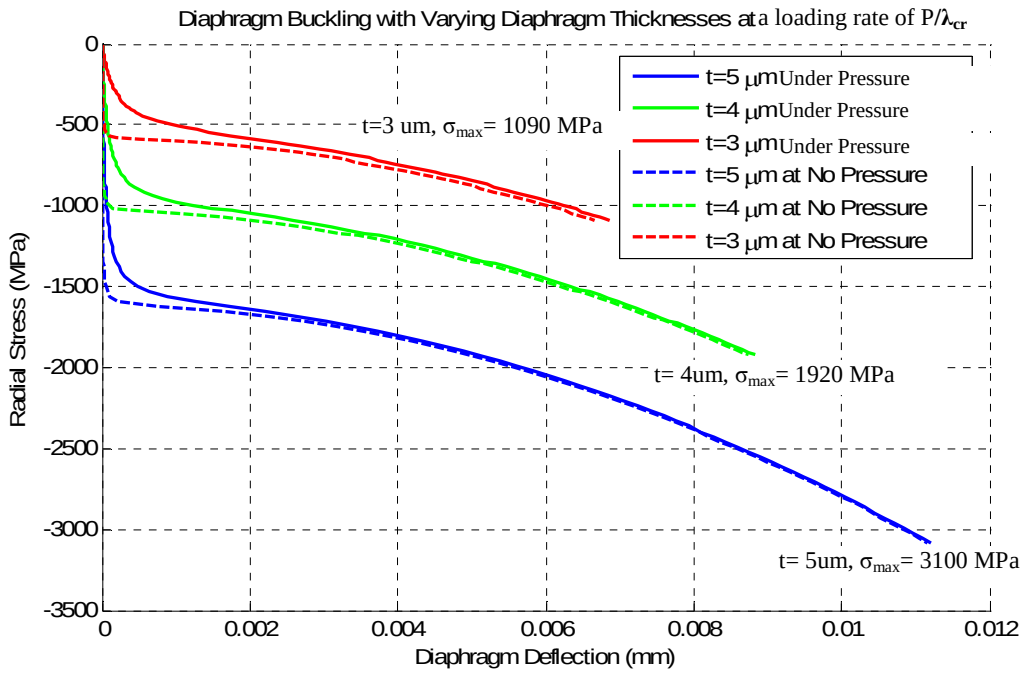
Diaphragm Buckling with Varying Diaphragm Thicknesses at a loading rate of P/λcr
t=5 μm Under Pressure
t=4 μm Under Pressure
t=3 μm Under Pressure
t=5 μm at No Pressure
t=4 μm at No Pressure
t=3 μm at No Pressure
t=3 um, σmax= 1090 MPa
t= 4um, σmax= 1920 MPa
t= 5um, σmax= 3100 MPa
Radial Stress (MPa)
Diaphragm Deflection (mm)
0
-500
-1000
-1500
-2000
-2500
-3000
-3500
0
0.002
0.004
0.006
0.008
0.01
0.012

(a)

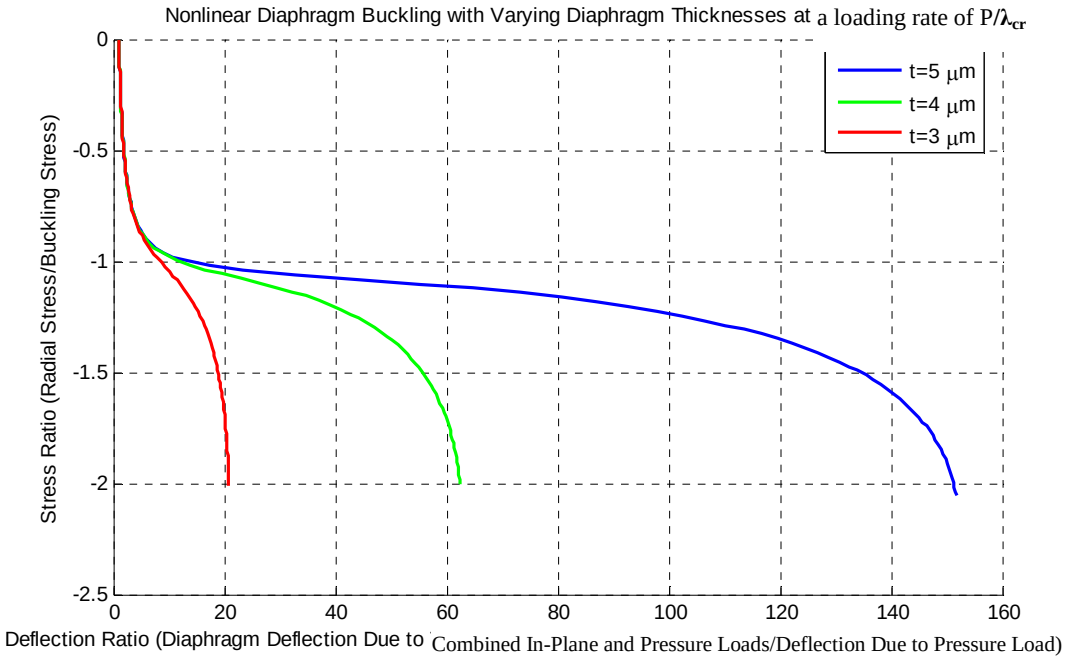
Nonlinear Diaphragm Buckling with Varying Diaphragm Thicknesses at a loading rate of P/λcr
t=5 μm
t=4 μm
t=3 μm
Stress Ratio (Radial Stress/Buckling Stress)
Deflection Ratio (Diaphragm Deflection Due to Combined In-Plane and Pressure Loads/Deflection Due to Pressure Load)
0
-0.5
-1
-1.5
-2
-2.5
0
20
40
60
80
100
120
140
160

(b)

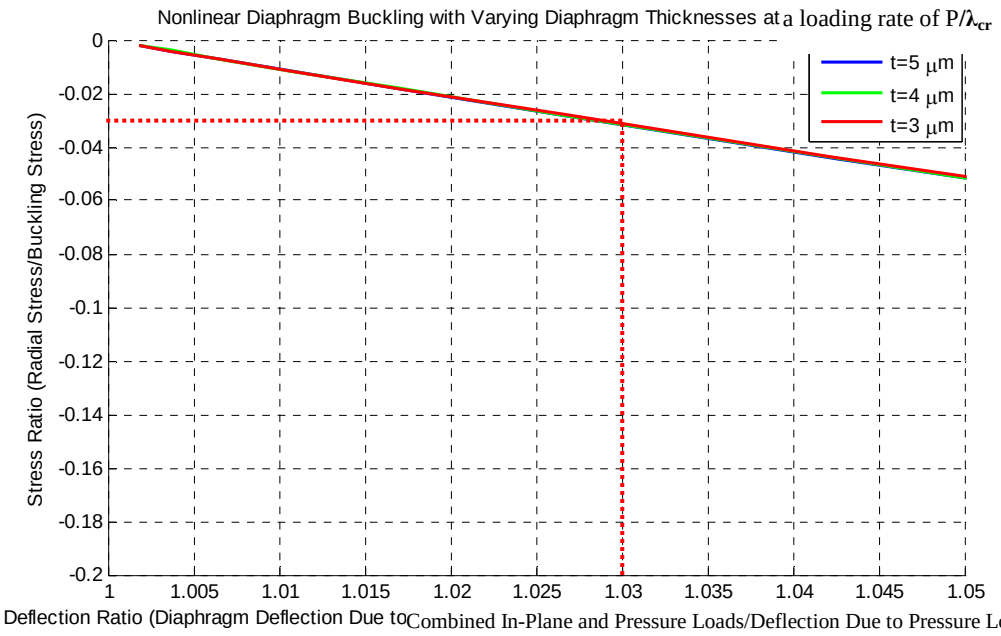

(c)

Fig. 3.10 (a) Nonlinear diaphragm deflection for *p*=4.6 bars increase of pressure, with proportional increase of in-plane compressive thermo-mechanical stresses up to the linear analytic buckling limit; for varying thicknesses, showing the nonlinearity before and after buckling. (b) Normalized diaphragm deflection curves. (c) A closer look at the normalized deflection curve showing the 'contamination limit'.

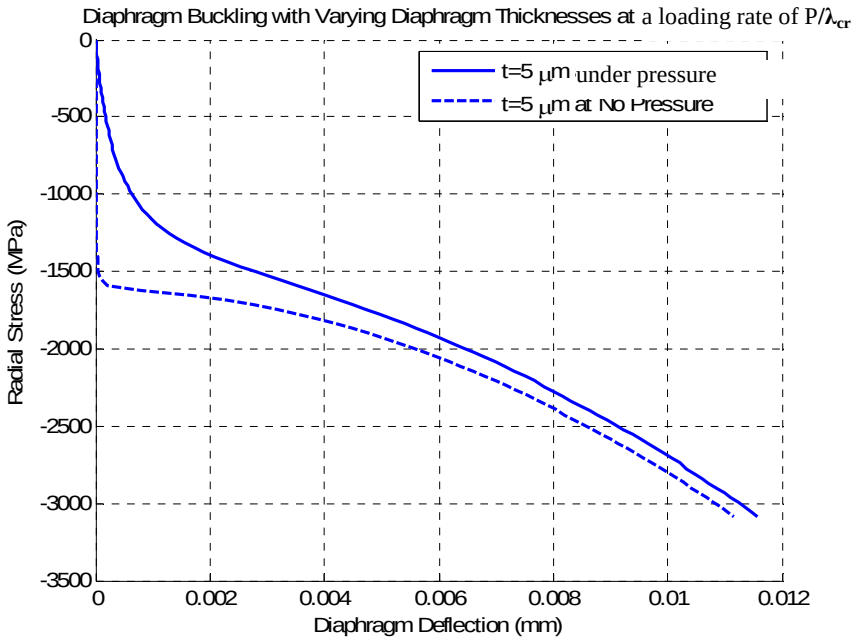
Diaphragm Buckling with Varying Diaphragm Thicknesses at a loading rate of P/λcr
t=5 μm under pressure
t=5 μm at No Pressure
Radial Stress (MPa)
0
-500
-1000
-1500
-2000
-2500
-3000
-3500
0
0.002
0.004
0.006
0.008
0.01
0.012
Diaphragm Deflection (mm)

(a)

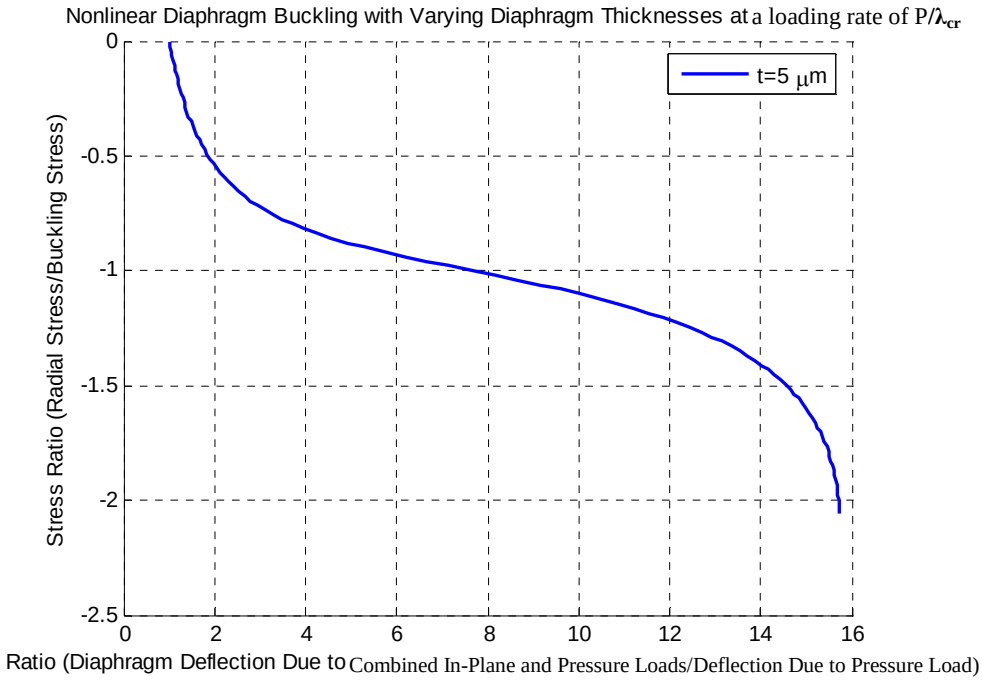
Nonlinear Diaphragm Buckling with Varying Diaphragm Thicknesses at a loading rate of P/λcr
t=5 μm
Stress Ratio (Radial Stress/Buckling Stress)
0
-0.5
-1
-1.5
-2
-2.5
0
2
4
6
8
10
12
14
16
Ratio (Diaphragm Deflection Due to Combined In-Plane and Pressure Loads/Deflection Due to Pressure Load)

(b)

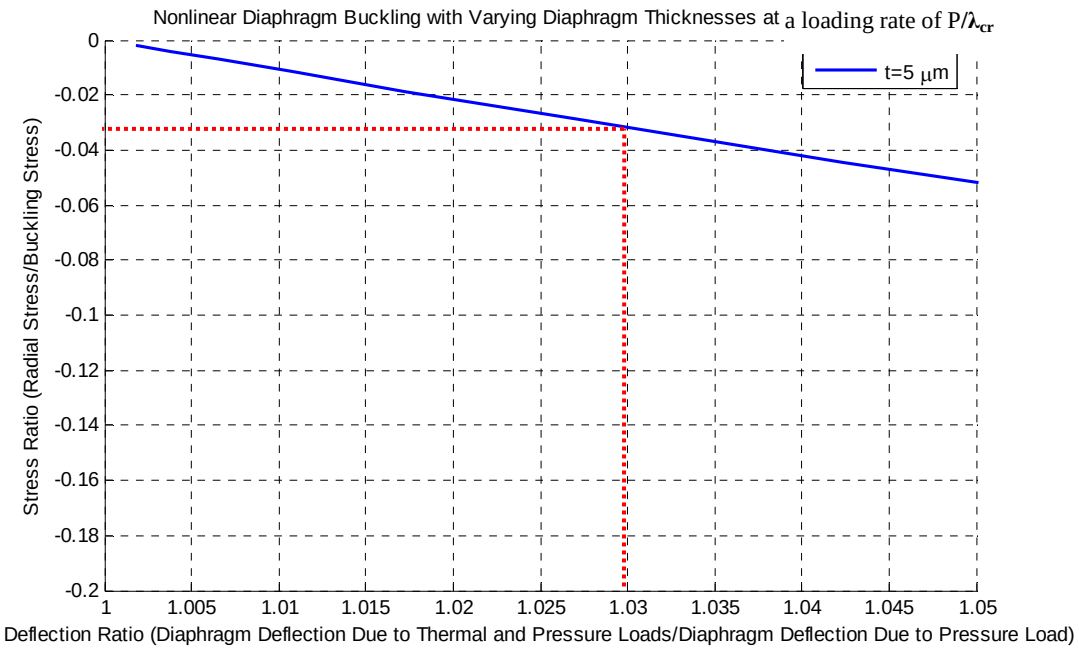

(c)

Fig. 3.11 (a) Nonlinear diaphragm deflection for *p*=46 bars increase of pressure, with proportional increase of in-plane compressive thermo-mechanical stresses up to the linear analytic buckling limit; for varying thicknesses, showing the nonlinearity before and after buckling. (b) Normalized diaphragm deflection curves. (c) A closer look at the normalized deflection curve showing the 'contamination limit'.

3.6.2 Sequential Change: Temperature Drop Followed by Pressure Loading

In many application environments, the FOPS will have to undergo a temperature drop to operating conditions and then experience pressure loading during pressure measurement. In order to recreate this sequential effect, the FOPS is analyzed under sequential loading of temperature drop (of various magnitudes below the stress-free temperature) followed by pressure loading.

The FOPS diaphragm is first subjected to a temperature drop which causes an initial deflection in the sensor's diaphragm due to the thermally-induced in-plane compressive stresses (produced as the outer casing shrinks relative to the diaphragm, due to the temperature drop). Then the diaphragm is placed under a pressure load. Five cases are examined, with the temperature drop varying from 0°C to -85°C below the stress-free temperature. The pressure is then monotonically increased to 100 bars. The nonlinear deflections for this loading sequence are examined for three cases of diaphragm thickness: t=3μm, t=4μm and t=5μm. The temperature drop is simulated by applying in-plane thermo-mechanical stresses estimated from Figure 3.5.

Fig.3.12 (a) illustrates the nonlinear deflections of a 3μm thick diaphragm under this sequential loading. The initial temperature-induced deflections are subtracted out since the FOPS sensor will output only the pressure-induced deflections. This figure shows that as the temperature-induced pre-deflection increases, the diaphragm stiffens more, thus increasing the nonlinearity in the pressure-induced deflection. Note that the diaphragm deflections for $\Delta T = 0\ ^{o}C$ in Figure 3.12(a) are slightly less than those presented earlier by Majeed at al [see Figure 2.8 of ref 9] due to the fact that here only the diaphragm of the FOPS is modeled, whereas in Fig. 2.8 of Ref 9, the entire FOPS assembly was analyzed. Figures 3.12 (b) and (c) illustrate the effect of this sequential loading as the diaphragm thickness is increased to 4μm and 5μm, respectively. As the diaphragm thickness is increased, the effects of the initial temperature drop are lessened.

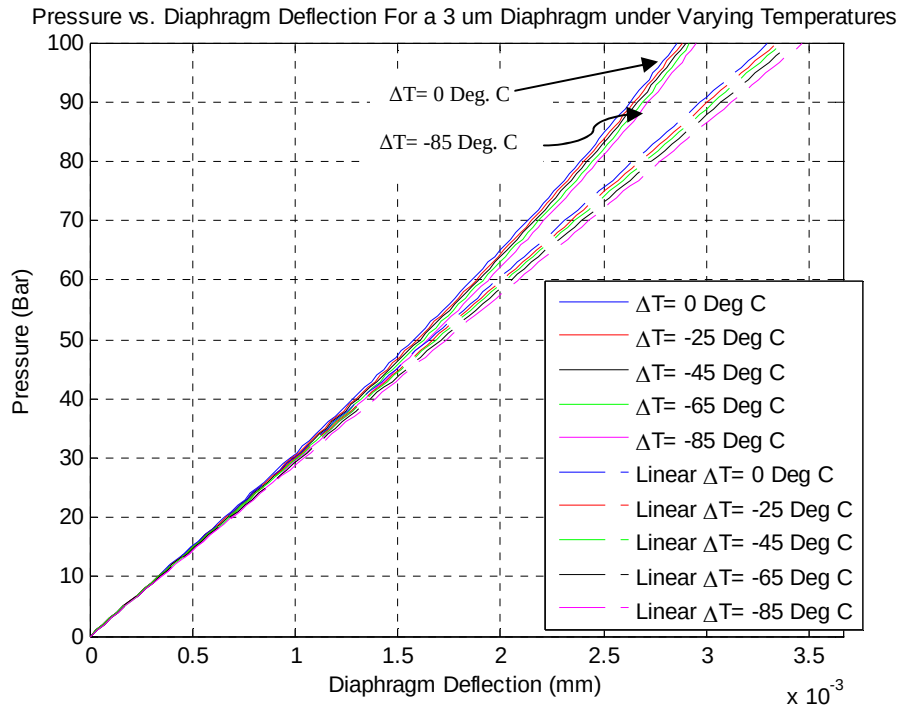
Pressure vs. Diaphragm Deflection For a 3 um Diaphragm under Varying Temperatures
ΔT= 0 Deg. C
ΔT= -85 Deg. C
Pressure (Bar)
Diaphragm Deflection (mm)
x 10^-3
ΔT= 0 Deg C
ΔT= -25 Deg C
ΔT= -45 Deg C
ΔT= -65 Deg C
ΔT= -85 Deg C
Linear ΔT= 0 Deg C
Linear ΔT= -25 Deg C
Linear ΔT= -45 Deg C
Linear ΔT= -65 Deg C
Linear ΔT= -85 Deg C

(a)

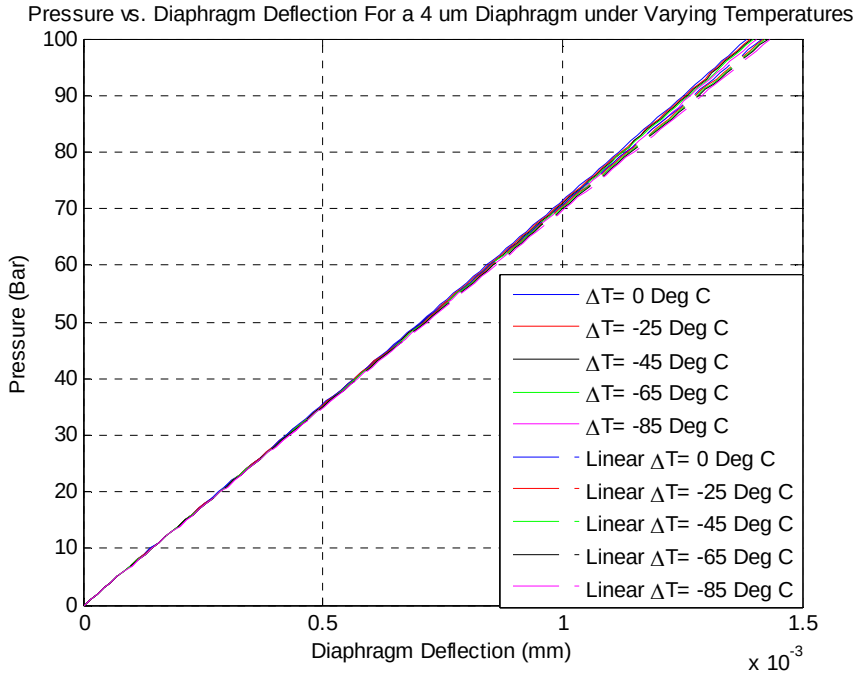
Pressure vs. Diaphragm Deflection For a 4 um Diaphragm under Varying Temperatures
Pressure (Bar)
Diaphragm Deflection (mm)
x 10^-3
ΔT= 0 Deg C
ΔT= -25 Deg C
ΔT= -45 Deg C
ΔT= -65 Deg C
ΔT= -85 Deg C
Linear ΔT= 0 Deg C
Linear ΔT= -25 Deg C
Linear ΔT= -45 Deg C
Linear ΔT= -65 Deg C
Linear ΔT= -85 Deg C

(b)

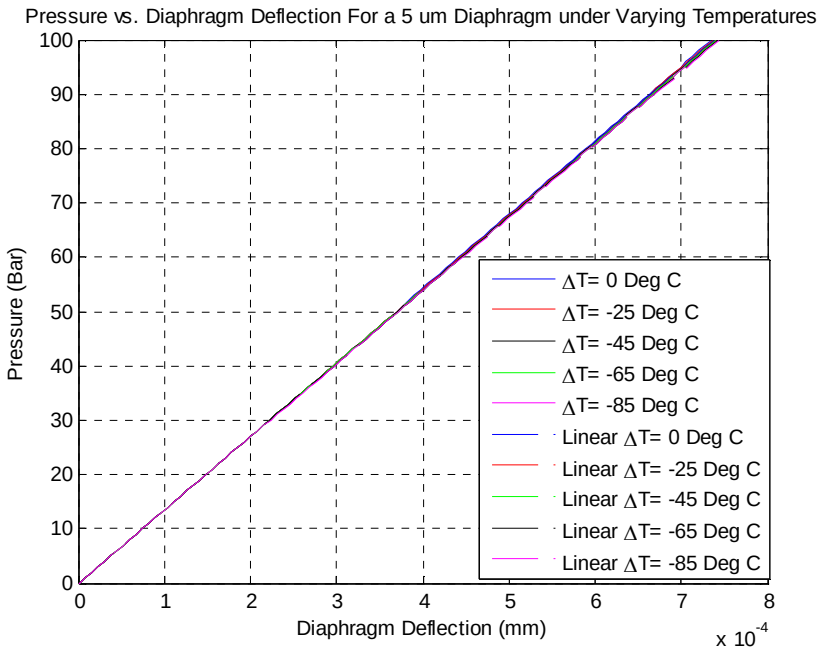

(c)

Fig.3.12. Nonlinear diaphragm deflection under sequential temperature drop (five cases: 0, -25, -45, -65, -85 deg C), followed by monotonic pressure loading to 100 bars, for (a) t=3μm, (b) t=4μm and (c) t=5μm.

As the temperature and pressure loadings are increased, an important factor that must be noted is the percent nonlinearity and the corresponding linearity limit that defines the static working range of the FOPS. Fig.3.13 shows the working pressure ranges based on 1%, 2% and 3% nonlinearity, for temperature drops up to -85 ^{o}C. For example, at a temperature drop of -85 ^{o}C, a 3μm diaphragm reaches 3% nonlinearity at about 20 bar pressure. So with this sequential loading, the working temperature and pressure range can be prescribed. Interestingly, the working pressure limit is not very sensitive to temperature drop, for the cases examined.

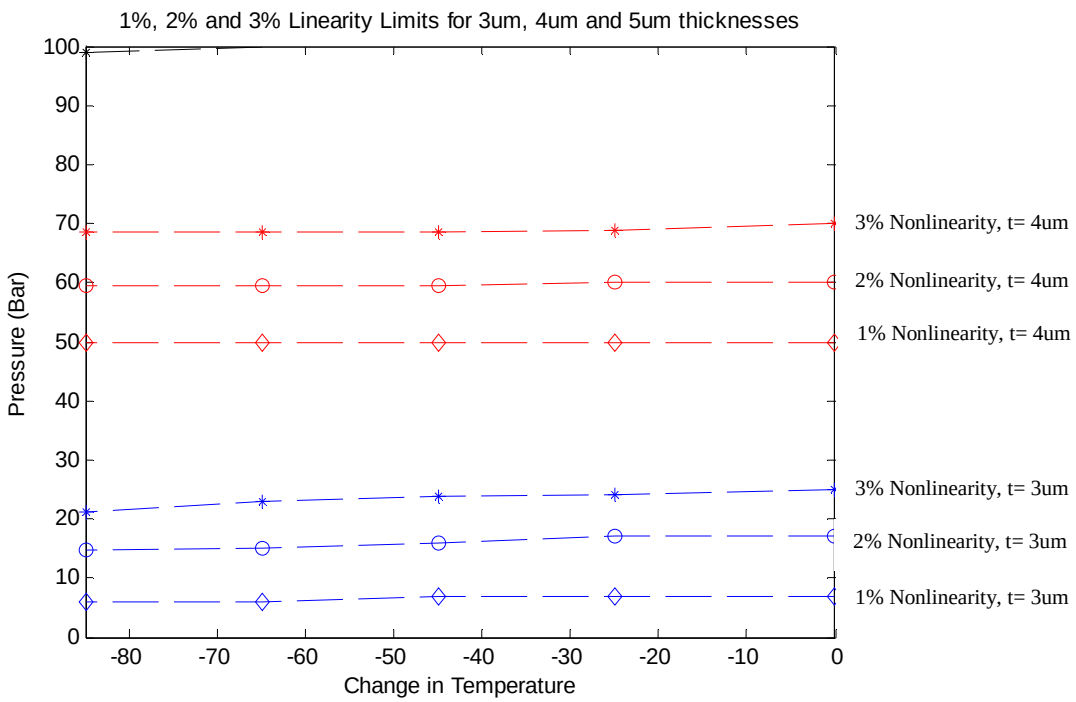

Fig. 3.13. Working pressure ranges for t=3µm, t=4µm and t=5µm, based on 1%, 2% and 3% nonlinearity.

Another important parameter that needs to be examined is the FOPS Calibration Factor, defined as the diaphragm deflection (µm) per unit pressure (bar) loading within the linear working range. This calibration factor is estimated from the initial linear tangent slope of the pressure-deflection curves in Figure 3.12, and plotted in Fig. 3.14. Once again, the calibration factors are found to be relatively insensitive to temperature for most of the cases examined, with the sensitivity increasing progressively as the operating temperature drops. As expected, the calibration factor becomes more sensitive to the operating temperature, as the diaphragm thickness decreases.

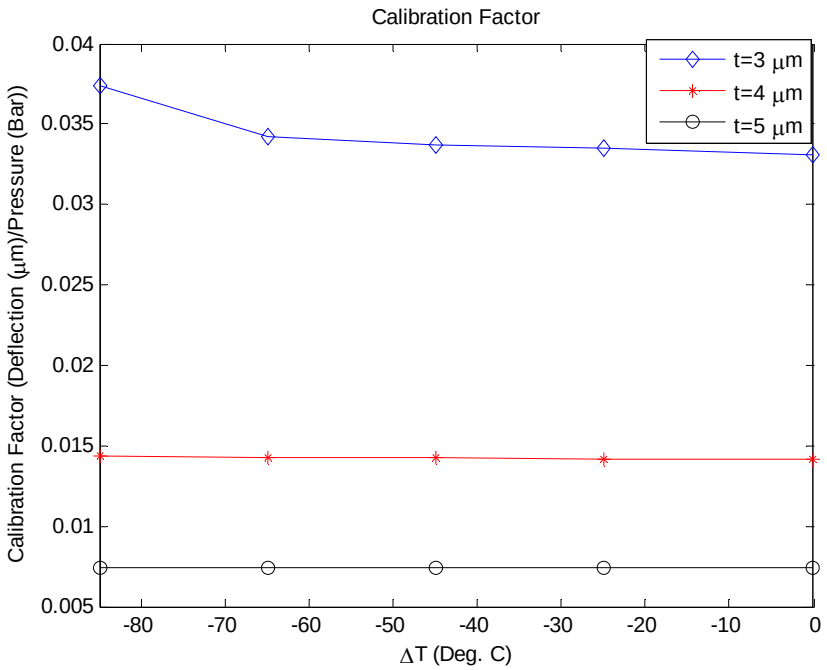

Fig. 3.14. Calibration factor (diaphragm deflection per unit pressure change within the linear limit), for t=3μm, t=4μm and t=5μm

3.7 Conclusions

In application environments, the FOPS will undergo not only a pressure load, but also temperature excursions. The resulting compressive, in-plane thermo-mechanical loads can generate diaphragm buckling, thus adding to the diaphragm deflection, and compromising the accuracy of the pressure measurement. In this study, the diaphragm was subjected to a proportional increase of pressure and in-plane thermally-induced compressive stress. This work shows that when the thermo-mechanical in-plane radial stress reaches 3% of the buckling strength of the diaphragm, the output of the FOPS is contaminated with a mixture of deflection due to both thermo-mechanical buckling and pressure-induced bending of the diaphragm

(acceptable threshold is defined here as 3% deviation from the purely pressure-induced deflection). The temperature and pressure combination, at which the radial stress reaches 3% of the critical buckling strength of the diaphragm, is defined as the lower 'contamination limit' of the FOPS (because past this limit the thermally-induced buckling deflection is more than 3% of the pressure-induced bending deflection). For example, a 3 µm thick diaphragm has a lower 'contamination limit' of about -16 MPa (corresponds to approximately -60 ^{o}C, based on the results in Figure 3.4) and 0.15 bar pressure (Fig. 3.12). Buckling calibration curves are provided in this study to allow users to find this lower 'contamination limit' for a range of diaphragm thickness for this FOPS.

Similarly, the lower 'linearity limit' of the FOPS at each pressure is defined by the temperature and pressure combination that causes 3% nonlinearity in the diaphragm deflection due to combined buckling and pressure. For example, close examination of the data in Figure 3.8 reveals that the lower 'linearity limit' of the 3 µm thick diaphragm studied in this FOPS occurs at a compressive radial stress of -67 MPa (corresponding to temperature lower than -150 Deg. C, based on the results in Figure 3.4) and 0.6 bar pressure.

The operating range of the FOPS is defined by the more stringent of these two ranges defined above. In the case discussed above, clearly the 'contamination limit' defines the operating range of the FOPS. It's worth noting that the operating pressure range for this case is only 0.15 bars (at -60 Deg C temperature, from Figure 3.4) compared to the operating range of 20 bar pressure in the absence of thermal loading. Clearly, a

proportional simultaneous drop in temperature significantly reduces the operating pressure range of the FOPS. As the thickness of the diaphragm increases, so does its operating range.

In many application environments, the FOPS will have to undergo a temperature drop to operating conditions and then experience pressure loading during pressure measurement. In order to recreate this sequential effect, the FOPS is analyzed under sequential loading of temperature drop (of various magnitudes below the stress-free temperature) followed by pressure loading. The FOPS diaphragm is first subjected to a temperature drop which causes an initial deflection in the sensor's diaphragm due to the thermally-induced in-plane compressive stresses (produced as the outer casing shrinks relative to the diaphragm, due to the temperature drop). Then the diaphragm is placed under a pressure load. Five cases are examined, with the temperature drop varying from 0°C to -85°C below the stress-free temperature. The pressure is then monotonically increased to 100 bars.

It is shown that for this particular temperature-pressure combination, as the temperature-induced pre-deflection increases, the diaphragm stiffens more, thus increasing the nonlinearity in the pressure-induced deflection and that as the diaphragm thickness is increased, the effects of the initial temperature drop are lessened. The working pressure ranges based on 1%, 2% and 3% nonlinearity, for temperature drops upto -85 ^{o}C are also shown along with the FOPS Calibration Factor (defined as the diaphragm deflection (μm) per unit pressure (bar) loading within the linear working range). The calibration factors and the nonlinearity limits

are found to be relatively insensitive to temperature drop for most of the cases examined, with the sensitivity increasing progressively as the operating temperature drops. Further studies are required to explore different combinations of non-proportional changes in temperature and pressure in order to explore the entire operating range of the FOPS.

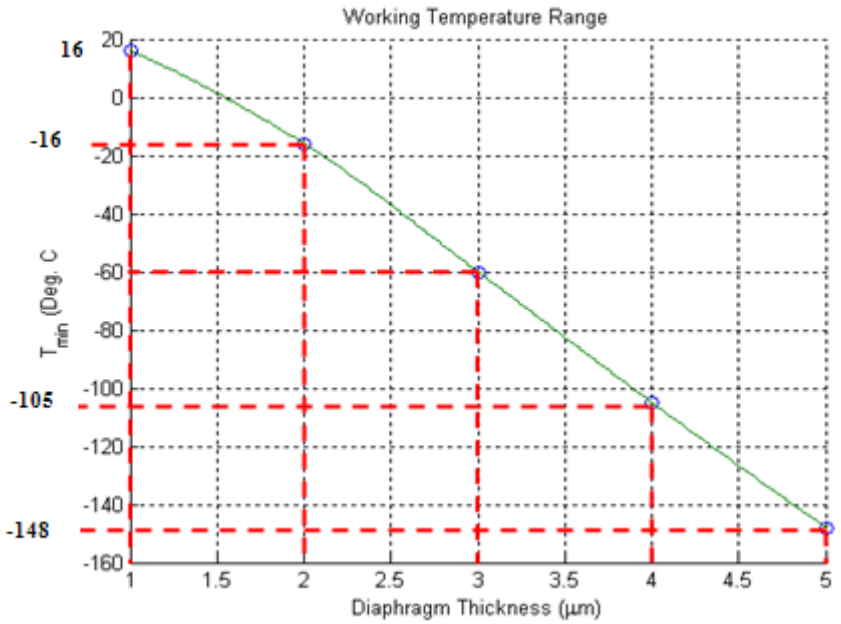

Fig. 3.15 Working temperature range for different diaphragm thicknesses from Figure 3.8 and Figure 3.4.

3.9 Acknowledgements

This research is funded in part by Pervasive Technology Engineering, LLC and in part by the State of Maryland through MIPS contract # 3837. The authors thank Dr. M. Eltoweissy from the company for providing technical assistance needed for the project.

3.10 References

[1] Shilpak, M., Dugundji, J., "Large deflections of clamped circular plates under initial tension and translation of membrane behavior," ASME Journal of Applied Mechanics Papers 65, 107-115 (1998)

[2] Yu, M., Balachandran, B., "Sensor diaphragm under initial tension: linear analysis," Experimental Mechanics Papers 45, 123-129 (2005)

[3] Zheng, N., Shi, C., Wang, D., Zhang, M., Liao, Y., "Diaphragm type fiber optic interferometric acoustic sensors, Optical Engineering," Papers 42, 2558-2562 (2003)

[4] Yu, M., Balachandran, B., "Acoustic measurements using fiber optic sensor system," Journal of Intelligent Material Systems and Structures Papers 14, 409-414 (2003)

[5] Yu, M., Long, X., Balachandran, B., "Sensor diaphragm under initial tension: nonlinear responses and design implications," Journal of Sound and Vibration Papers 312, 39-54(2005)

[6] Al-Bassyiouni, M., Yu, M., Balachandran, B., Oh, J., "Fiber optic sensors for active acoustic control,"Proc. SPIE 4693, 39-54 (2005)

[7] Ettouhami, A., Essaid, A., Ouakrim, N., Michel, L., Limouri, M., "Thermal Buckling of Silicon Capacitative Pressure Sensor," Journal of Sensors and Actuators A 57 167-171(1996)

[8] Parkus, H., [Thermoelasticity] Springer, New York, 2nd Ed. 1976, pp 47-63

[9] Majeed, Y., Al-Bassiyouni, M., Dasgupta, A., "Design Optimization of Fiber Optic Sensors," Optical Society of America (2009)

[10] Soedel, W., [Vibrations of shells and plates], Marcel Dekker, New York, 1993

[11] Kalamkarov, A., MacDonald, D., Fitzgerald, S., Georgiades, A., “Reliability assessment of pultred FRP reinforcements with embedded fiber optic,” Composite Structures Paper 50, 69-78 (2000)

[12] Timoshenko, S., [Strength of Materials], Krieger Pub Co , 1976,

[13] Timoshenko, S., [Theory of Plates and Shells], McGraw-Hill, New York, 1940

[14] Peterson, K.E., “Silicon as a Mechanical Material,” Proc IEEE 70 5 420-457(1982)

[15] Ding, X., Ko, W., Niu, Y., He, W, “A Study on Silicon Diaphragm Buckling,” Tech. Dig., IEEE, Hilton head Islan, SC, 128-207(1990)

Chapter 4: Summary

The main conclusions of this thesis and contributions to this project are presented and discussed here, along with recommendations for future work.

4.1 Conclusions and Discussions

In this study, the design methodology for the diaphragm of a fiber optic pressure sensor under combinations of steady-state pressure and temperature are investigated. Due to these conditions, several failure mechanisms may affect the structural and optical characteristics of the sensor, such as nonlinear displacement of the diaphragm, buckling of the diaphragm, cracks in the diaphragm, high residual stresses in the optical fiber and deformations and failure in the epoxy sealant between the optical fiber and the steel casing. With the aid of linear and nonlinear FEA, this study investigated the severity of selected failure mechanisms in the sensor (nonlinear diaphragm deflection, diaphragm fracture and diaphragm buckling).

In the first part of the study the effect of pressure loading at ambient temperatures was investigated. For maximum sensitivity, it is ideal to have as thin a diaphragm as possible. However, as the thickness of the diaphragm is reduced, the stresses developed at the periphery of the diaphragm due to the deflection become an important factor. The work conducted shows that the reliability in terms of these stresses produced in the diaphragm due to an external pressure load are not critical for

any practical pressure range. The stresses developed in the diaphragm are much below the fracture strength of silicon even for very small diaphragm thicknesses.

However, as the diaphragm thickness is reduced and the pressure loading is increased, the diaphragm deflections exceed the linear range. As the diaphragm deflection approaches 30% of its thickness, the linearized response is no longer valid and nonlinear effects have to be taken into consideration. It was shown that nonlinearity plays a critical role in the design and limits the operating pressure range and the allowable minimum thickness of the diaphragm. As expected, the pressure range decreases as the diaphragm thickness reduces. Using the nonlinear calibration curves provided in this work, sensors can be designed using 1%-3% nonlinearity criteria, to assess their working pressure range.

In application environments, the FOPS will undergo not only a pressure load, but also temperature excursions. The second part of the study examines the effect of combined temperature and pressure loading and explores the diaphragm deflections under different combinations of temperature drop and pressure loading. First the study analyzes nonlinear diaphragm deflections under simultaneous, proportional changes in temperature and pressure, for different proportionality ratios. This represents application conditions where the FOPS will experience simultaneous changes in temperature and pressure. Then the nonlinear diaphragm deflection under sequential changes, with various magnitudes of temperature drop followed by monotonic pressure loading is analyzed. This represents application conditions where

the FOPS will have to measure pressure at steady ambient temperatures that are below the stress-free temperature.

The compressive, in-plane thermo-mechanical loads can generate diaphragm buckling, thus adding to the diaphragm deflection, and compromising the accuracy of the pressure measurement. First, the diaphragm was subjected to a proportional increase of pressure and in-plane, thermally-induced, compressive stress. This work shows that under this proportional loading, when the thermo-mechanical in-plane radial stress reaches 3% of the buckling strength of the diaphragm, the output of the FOPS is contaminated with a mixture of deflection due to both thermo-mechanical buckling and pressure-induced bending of the diaphragm The temperature and pressure combination, at which the radial stress reaches 3% of the critical buckling strength of the diaphragm, is defined as the lower 'contamination limit' of the FOPS. Buckling calibration curves are provided in this study to allow users to find this lower 'contamination limit' for proportional loading, for a range of diaphragm thickness for this FOPS.

Also, the lower 'linearity limit' of the FOPS at each pressure is defined by the temperature and pressure combination that causes 3% nonlinearity in the diaphragm deflection due to proportional increase in combined buckling and pressure examined in this study. The operating range of the FOPS is defined by the more stringent of these two ranges. It is shown that a drop in temperature significantly reduces the operating pressure range of the FOPS. As the thickness of the diaphragm increases, so does its operating range. This study demonstrates the method to estimate these

operating ranges for a particular proportional combination of pressure and temperature changes.

But, in many application environments, the FOPS will have to undergo a temperature drop to operating conditions and then experience pressure loading during pressure measurement. In order to recreate this sequential effect, the FOPS is analyzed under sequential loading of temperature drop (of various magnitudes below the stress-free temperature) followed by pressure loading. The FOPS diaphragm is first subjected to a temperature drop which causes an initial deflection in the sensor's diaphragm due to the thermally-induced in-plane compressive stresses (produced as the outer casing shrinks relative to the diaphragm, due to the temperature drop). Then the diaphragm is placed under a pressure load. Five cases are examined, with the temperature drop varying from 0°C to -85°C below the stress-free temperature. The pressure is then monotonically increased to 100 bars.

It is shown that for this particular temperature-pressure combination, as the temperature-induced pre-deflection increases, the diaphragm stiffens more, thus increasing the nonlinearity in the pressure-induced deflection and that as the diaphragm thickness is increased, the effects of the initial temperature drop are lessened. The working pressure ranges based on 1%, 2% and 3% nonlinearity, for temperature drops upto -85 ^{o}C are also shown along with the FOPS Calibration Factor (defined as the diaphragm deflection (µm) per unit pressure (bar) loading within the linear working range). The calibration factors and the nonlinearity limits are found to be relatively insensitive to temperature drop for most of the cases

examined, with the sensitivity increasing progressively as the operating temperature drops. Further studies are required to explore different combinations of non-proportional changes in temperature and pressure in order to explore the entire operating range of the FOPS.

4.2 Major Contributions and Future Work

The major contributions and suggestions for future work are outlined below:

- In this thesis, linear as well as nonlinear design sensitivity of a fiber optic pressure sensor (FOPS) under thermal and pressure loads were explored
- In previous work, FOPS have been designed with respect to the sensitivity of the sensors by optimizing the thickness of the diaphragm for maximum deflection. This study quantitatively investigates the tradeoffs between increasing the sensitivity of the sensor and limiting the operating range of the FOPS, due to the nonlinearity of the diaphragm, as the thickness of the diaphragm is reduced and the external pressure loading is increased. Calibration curves of the diaphragm deflection under a range of working pressure loads and diaphragm thicknesses are provided for linear as well as nonlinear working range for end-users.
- Another important contribution of this thesis is the analysis of the in-plane compressive stresses generated in the FOPS diaphragm due to drop in the application temperature, and the resulting post-buckling deformations of the diaphragm.

- Not only is the FOPS analyzed under a temperature drop, but also an external pressure load is added in order to recreate its working environment.
    - First the nonlinear diaphragm deflections under simultaneous, proportional changes in temperature and pressure, for different proportionality ratios. This represents application conditions where the FOPS will experience simultaneous changes in temperature and pressure
        - Outcome is an assessment of the temperature limits of the FOPS with different diaphragm thicknesses at different pressures; based on contamination and nonlinearity of the pressure-induced deflections due to the additional buckling-induced deformations.
    - Then nonlinear diaphragm deflection under sequential changes, with various magnitudes of temperature drop followed by monotonic pressure loading. This represents application conditions where the FOPS will have to measure pressure at steady ambient temperatures that are below the stress-free temperature.
        - Outcome is an assessment of the working pressure ranges based on 1%, 2% and 3% nonlinearity, for temperature drops upto -85 ^{o}C along with a Calibration Factor (defined as the diaphragm deflection (µm) per

unit pressure (bar) loading within the linear working range)

- Future Work:
  - This study shows the methodology of designing the FOPS for different combinations of temperature and pressure. First, a particular proportional combination of pressure and temperature loading has been used to show the methodology. Then, the nonlinear diaphragm deflection under sequential changes, with various magnitudes of temperature drop followed by monotonic pressure loading is analyzed in order to represents application conditions where the FOPS will have to measure pressure at steady ambient temperatures that are below the stress-free temperature. Further studies are required to explore more of these operating ranges for different thicknesses and for other combinations of non-proportional changes in temperature and pressure.

  - This work has not considered the effects of environmental dynamic loading on the FOPS. These dynamic loadings, which include vibration, shock and drop loadings, may affect the sensitivity of the sensor. In addition, the effects of dynamic pressure loading have to be

considered. Other phenomenon such as lifetime and phase difference must also be studied.

Appendix A: Sensor Modeling in Pro-Engineer

FEA Model

The FOPS, Fig. A, was modeled using two different techniques to optimize the analysis. First we modeled the sensor using Pro-Engineer and imported the design in to ANSYS for Finite Element Analysis. The methods of designing in Pro-Engineer are described in this appendix.

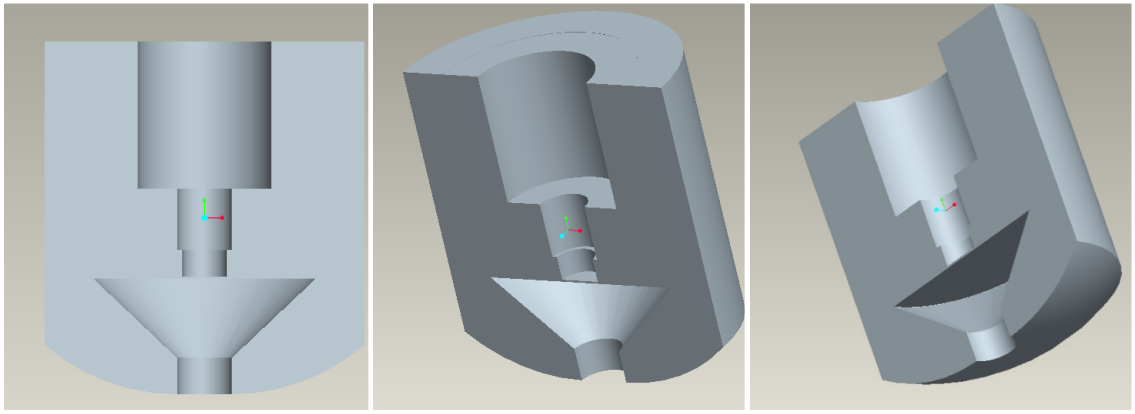

(a) (b) (c)

Fig. A1(a) FOPS model in Pro-Engineer. (b) and (c) are angled views of the modeled FOPS

Material Properties

The FOPS consists of three different materials. The outer shield, which encompasses the probe housing, is made from steel. The probe housing and the fiber are of silicon material. The material properties are listed in the Table A1 below and the different material locations are illustrated in Fig. 2(b) with different colors.

Table A1. List of material properties used in the FEA model.

	Steel (Shield)	Silicon (Probe Housing)	Adhesive
Density (kg/m^3)	7820	2330	1720
Poisson's ratio	0.27	0.28	0.28
Young's modulus (GPa)	200	112.4 - 165	2.26
Coefficient of thermal expansion (K^{-1})	15.2e-6	3.2e-6	191e-6

FEA Results

As mentioned above, the point of interest is the sensor diaphragm shown in Fig. 1, Sec. 2.1. The diaphragm nominal dimensions are 100μm diameter and 5μm thickness. When applying 1.0 bar pressure, the resulting maximum deformation is noted to be 9.1nm at the geometric center of the diaphragm as shown in Fig. A2 (a). The maximum principal stress is 6.9 MPa and it occurs at the diaphragm circumference as shown in Fig. A2 (b).

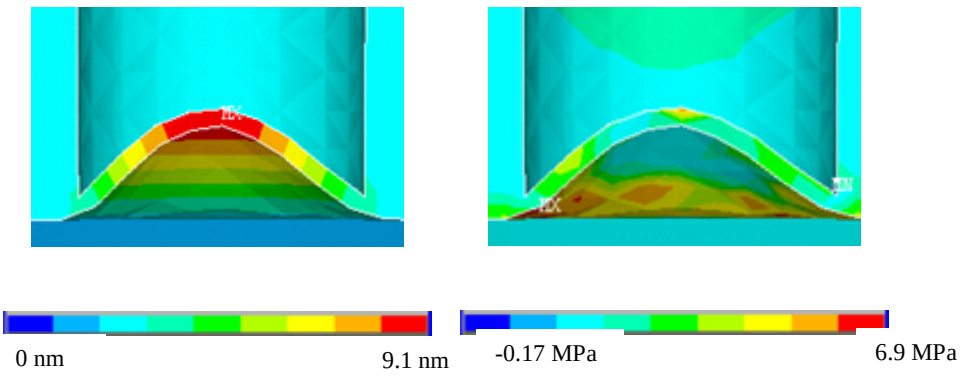

(a) (b)

Fig. A2. (a) Deflection of the sensor diaphragm under pressure loading of 1.0 bar scaled by 5K and (b) principal stresses on the diaphragm

REFERENCES

[1] Shilpak, M., Dugundji, J., “Large deflections of clamped circular plates under initial tension and translation of membrane behavior,” ASME Journal of Applied Mechanics Papers 65, 107-115 (1998)

[2] Yu, M., Balachandran, B., “Sensor diaphragm under initial tension: linear analysis,” Experimental Mechanics Papers 45, 123-129 (2005)

[3] Zheng, N., Shi, C., Wang, D., Zhang, M., Liao, Y., “Diaphragm type fiber optic interferometric acoustic sensors, Optical Engineering,” Papers 42, 2558-2562 (2003)

[4] Yu, M., Balachandran, B., “Acoustic measurements using fiber optic sensor system,” Journal of Intelligent Material Systems and Structures Papers 14, 409-414 (2003)

[5] Yu, M., Long, X., Balachandran, B., “Sensor diaphragm under initial tension: nonlinear responses and design implications,” Journal of Sound and Vibration Papers 312, 39-54(2005)

[6] Al-Bassyiouni, M., Yu, M., Balachandran, B., Oh, J., “Fiber optic sensors for active acoustic control,”Proc. SPIE 4693, 39-54 (2005)

[7] Ettouhami, A., Essaid, A., Ouakrim, N., Michel, L., Limouri, M., “Thermal Buckling of Silicon Capacitative Pressure Sensor,” Journal of Sensors and Actuators A 57 167-171(1996)

[8] Parkus, H., [Thermoelasticity] Springer, New York, 2nd Ed. 1976, pp 47-63

[9] Majeed, Y., Al-Bassiyouni, M., Dasgupta, A., “Design Optimization of Fiber Optic Sensors,” Optical Society of America (2009)

[10] Soedel, W., [Vibrations of shells and plates], Marcel Dekker, New York, 1993

[11] Kalamkarov, A., MacDonald, D., Fitzgerald, S., Georgiades, A., "Reliability assessment of pultred FRP reinforcements with embedded fiber optic," Composite Structures Paper 50, 69-78 (2000)

[12] Timoshenko, S., [Strength of Materials], Krieger Pub Co , 1976,

[13] Timoshenko, S., [Theory of Plates and Shells], McGraw-Hill, New York, 1940

[14] Peterson, K.E., "Silicon as a Mechanical Material," Proc IEEE 70 5 420-457(1982)

[15] Ding, X., Ko, W., Niu, Y., He, W, "A Study on Silicon Diaphragm Buckling," Tech. Dig., IEEE, Hilton head Islan, SC, 128-207(1990)

[16] M. Yu, Fiber-Optic Sensors for Acoustic Measurements, PhD Dissertation, University of Maryland, College Park, MD, 2002

[17] Petersen, K.E., Silicon as a mechanical material, *Proc. IEEE.*, Vol. 70, No. 5, 1982